Residence time distributions in sinuosity-driven hyporheic zones and their biogeochemical effects

Jesus D. Gomez,[1] John L. Wilson,[1] and M. Bayani Cardenas[2]

[1] Hyporheic exchange plays a key role in the biogeochemical evolution of water and in ecosystem functioning at the local, reach, and watershed scales. Residence time is a fundamental metric to describe the possible transformation taking place in this exchange zone. With this in mind, we use a simple conceptual model to explore the residence time distributions (RTDs) of sinuosity-driven hyporheic zones (HZs) and to discriminate the individual effect of sinuosity (σ), valley slope (J_x), hydraulic conductivity (K), aquifer dispersivity (α_L), and the biogeochemical timescales (BTSs) that characterize the degradation of dissolved organic carbon in these hydrologic systems. We find that RTDs are characterized by one early mode and a late time power law behavior. For a given aquifer dispersivity, the shape of these distributions is stretched or compressed by changes in J_x, K, and σ, having a strong influence on the net biogeochemical transformations within the HZ. Using BTSs proposed in previous studies and sensitivity analyses, we show the potential of σ, J_x, and K to classify meander HZs as net sinks of nitrates or only modulators of the residence times in the subsurface where nitrate reduction is negligible. These findings can be used as predictive tools to quantify the potential of meanders as biogeochemical reactors at the watershed scale with the aid of remote sensing data and GIS processing techniques. These tools can guide experimental design, suggesting important locations to visit, sample, and/or instrument. Also, hyporheic restoration projects can use them for initial site selection and design of channel modifications.

1. Introduction

[2] Hyporheic exchange, the local scale interaction between rivers and their surrounding sediment, leads to bidirectional transport of mass (e.g., water, solutes, and colloids), energy (e.g., heat), and living organisms (e.g., bacteria and viruses). As a result of these transport processes, hyporheic zones (HZs) play a key role in the biogeochemical evolution of water and in ecosystem functioning at the local, reach, and watershed scales [*Hill*, 1997; *Jones and Mulholland*, 2000; *Mulholland et al.*, 2008; *Böhlke et al.*, 2009]. For example, HZs are associated with hot spots for transformation and assimilation of nutrients [*Dahm et al.*, 1998; *Baker et al.*, 1999; *Lautz and Fanelli*, 2008; *Mulholland et al.*, 2008; *Boano et al.*, 2010a; *Zarnetske et al.*, 2011a, 2011b; *Bardini et al.*, 2012], buffering of contaminants [*Fuller and Harvey*, 2000; *Gandy et al.*, 2007], modulation of water temperature [*Poole and Berman*, 2001; *Arrigoni et al.*, 2008], and the distribution and abundance of organisms living within the river corridor [*Valett et al.*, 1993; *Brunke and Gonser*, 1997; *Boulton et al.*, 1998].

[3] Recent experimental and modeling studies show that residence time (RT) can be used as a proxy for the biogeochemical potential of HZs at the scales involved in sinuosity-driven hyporheic exchange [e.g., *Pinay et al.*, 2009; *Boano et al.*, 2010a; *Zarnetske et al.*, 2011a]. The capacity and efficiency of the hyporheic zone to drive biogeochemical transformations is a complex function of (1) temperature, (2) abundance and supply of reactive species (e.g., DO, DOC, nitrogen, and phosphorous), (3) hydraulic and chemical heterogeneity, and (4) the net flow and transport characteristics which are all encapsulated by the residence time distribution (RTD). In general, it is hard to discriminate the individual contribution of these factors; most studies that do so are limited to small-scale batch and column experiments and 1-D and 2-D simulations [*Angley et al.*, 1992; *Estrella et al.*, 1993; *Brusseau et al.*, 1999a, 1999b; *Li et al.*, 2001; *Park et al.*, 2001; *Gu et al.*, 2007; *Bardini et al.*, 2012]. Conclusions from these small-scale studies are not always transferable to sinuosity-driven hyporheic exchange, which occurs over spatial scales of the order of 1–1000 m and over timescales from hours to years [*Revelli et al.*, 2008; *Cardenas*, 2008a, 2008b; *Tonina and Buffington*, 2009; *Buffington and Tonina*, 2009].

[4] *Pinay et al.* [2009] found significant correlation between the concentrations of solutes involved in the denitrification process and hyporheic water residence time for two meandering study sites in Alaska, USA. They observed

[1]Department of Earth and Environmental Science, New Mexico Institute of Mining and Technology, Socorro, New Mexico, USA.
[2]Department of Geological Sciences, University of Texas at Austin, Austin, Texas, USA.

Corresponding author: J. D. Gomez, Department of Earth and Environmental Science, New Mexico Institute of Mining and Technology, 801 Leroy Pl., MSEC 208, Socorro, NM 87801, USA. (jdgomez@nmt.edu)

an exponential relationship between nitrate N removal and travel time through the HZ. *Zarnetske et al.* [2011a] studied the dynamics of nitrate production and removal in a gravel bar in western Oregon, USA. Their observations suggest that the transition between net nitrification and denitrification is a function of residence time and exhibits a threshold behavior. Using a mathematical modeling approach, *Boano et al.* [2010a] explored the effect of flow and residence times on the biogeochemical zonation of meander hyporheic zones. They linked the physical findings of *Revelli et al.* [2008] with a biogeochemical model for the degradation of organic carbon [*Hunter et al.*, 1998]. Concentration patterns for different constituents in a sequence of redox reactions were compared to characteristic residence times in the meander neck and apex, demonstrating the importance of residence time on biogeochemical evolution. The degradation of organic carbon in the neck was small due to short residence times, while at the apex, where the residence times were longer, most of the hierarchical reaction processes were completed, leading to full degradation of organic carbon.

[5] The findings of these three observational and modeling studies suggest that the complex biogeochemical potential of the HZ can be effectively evaluated in the context of residence times. Moreover, they suggest the possibility of introducing simple parameterizations to discern biogeochemical hot spots at the watershed scale [e.g., *Buffington et al.*, 2004; *Buffington and Tonina*, 2009]. One idea is to predict the potential for exchange and transformation in terms of simple geomorphic parameters that can be easily obtained or calculated. For the case of sinuosity-driven hyporheic exchange, which is the focus of this work, valley slope and sinuosity satisfy this requirement. From an observational point of view, these predictive tools can guide experimental design, suggesting important locations to visit, sample, and/or instrument. Similarly, from the perspective of river and hyporheic restoration of impaired fluvial systems, these tools can guide the initial site selection and design of channel modifications. In fact, recent efforts to develop a deeper understanding of hyporheic exchange at different spatiotemporal scales [e.g., *Jones and Mulholland*, 2000; *Buss et al.*, 2009] have been partially driven by the necessity to establish an adequate framework to quantify and predict the benefits of hyporheic restoration [*Boulton et al.*, 2010; *Hester and Gooseff*, 2010, 2011]. A common restoration practice is the increase of planform complexity by increasing sinuosity, aiming to increase the residence time of water in both the channel reach and the HZ, improve the opportunity for chemical reactions and microbiological activity, redistribute channel sediments, augment habitat diversity, and modify riparian vegetation.

[6] In this article, we explore the following questions: (1) what are the main characteristics of RTDs for sinuosity-driven HZs, (2) can we find simple relationships between channel sinuosity, valley slope, hydraulic conductivity, and the characteristics of these RTDs, and (3) what is the potential role of the RTD's shape in explaining the biogeochemical evolution of hyporheic water? We answer these questions using the mathematical model for flow proposed by *Cardenas* [2009a] and elaborate on the findings of *Cardenas* [2009a, 2009b] and *Boano et al.* [2006], who only focused on the amount of exchange created by these geomorphic features and did not explore the characteristics of residence times or their effect on the biogeochemical evolution of hyporheic water. Previous works have explored the RTDs of sinuosity-driven hyporheic zones using a morphodynamic model and a particle tracking method [*Revelli et al.*, 2008; *Boano et al.*, 2010a]. We expand on these works by exploring a broader range of morphologies characterized by valley slope, hydraulic conductivity, and channel sinuosity. Furthermore, we link the biogeochemical model proposed by *Boano et al.* [2010a] with the modeled RTDs to evaluate the biogeochemical potential of this lateral HZ. This is a useful methodology to characterize the biogeochemical effect of hyporheic exchange that can be used in HZs driven by different geomorphic features such as riffle-pool sequences, dunes, and logs [e.g., *Storey et al.*, 2003; *Sawyer et al.*, 2012; *Bardini et al.*, 2012]. With our proposed conceptual model, we find that water leaving the HZ and returning to the stream has RTDs characterized by one main characteristic timescale (CTS), i.e., the mode of the RTD, and a late time power law behavior. As a result, moments of the distribution are poor descriptors for the range of residence times observed in the HZ and lead to biased estimates of the time that chemicals in the hyporheic water have to react within this zone. The mode CTS is inversely proportional to the valley slope and hydraulic conductivity and increases in a nonlinear fashion with sinuosity and aquifer dispersivity, reaching an asymptotic value for large sinuosities. On the other hand, the importance of the late time power law tail of the distribution, as reflected by the area under the curve, is independent of the valley slope and hydraulic conductivity, but increases as sinuosity and aquifer dispersivity decrease. For a given aquifer dispersivity, changes in valley slope, hydraulic conductivity, and sinuosity stretch or compress the RTD, resulting in potentially important changes of the HZ's biogeochemical zonation. The importance of these changes also depends on characteristic biogeochemical timescales (BTSs).

[7] The effect of older water recharged in upstream meanders is taken into account, and its contribution to the hyporheic zone studied is explored. For this work, we assume a homogeneous system with neutral conditions (the river has no net gain or loss); however, future work will concentrate on subsurface heterogeneity, preferential flow paths, transient flow, and contributions from local, intermediate, and regional groundwater sources (i.e., gaining or losing streams). The stream channel is conceptualized as an idealized sinusoidal curve with linearly varying hydraulic head, and the values of valley slope and channel sinuosity explored are consistent with the ones used by *Cardenas* [2009a, 2009b]. The planimetric scenarios explored cover a wide range of meandering rivers found in natural systems [*van den Berg*, 1995]. The structure of the article is as follows: first, we introduce the mathematical model for the vertically integrated flow and evolution of RTDs, then patterns of residence time distributions and their moments are presented and discussed in light of implications for both the HZ's biogeochemical potential and restoration practices, and finally, general conclusions are drawn.

2. Methods

2.1. Groundwater Flow

[8] The hydrologic system is conceptualized as a generic alluvial valley, which is characterized by a meandering river that fully penetrates the shallower alluvium and overlies an older, horizontal, low-permeability river deposit (see Figure 1a). Laterally, the valley is constrained by hillslopes. This system is modeled as a vertically integrated aquifer. The
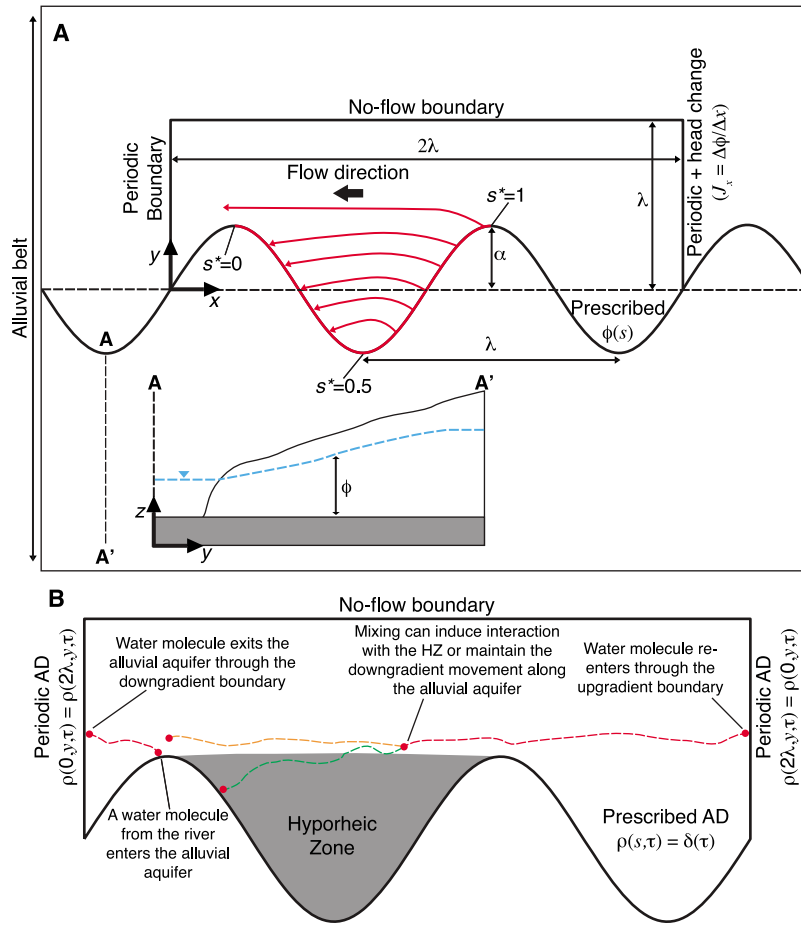
Figure 1. (a) Schematic representation of the alluvial system. The domain used for the mathematical model assumes that the system is axially symmetric and the meanders repeat periodically downstream, encompassing two periods in the downstream direction and one period across the alluvial belt. The red boundary corresponds to the meander used for the analysis, where flux-weighted RTDs are analyzed. (b) Approach used to account for the contribution of water through the lateral boundaries of the domain. A periodic boundary condition is used to account for an upgradient cycle of the domain. This assumption involves more characteristic timescales in the modeled RTDs.

alluvial aquifer, which is a homogeneous and isotropic porous medium, is bounded by a fully penetrating sinusoidal river and represented by a two-dimensional domain (see Figure 1a and *Cardenas* [2009a, 2009b]). Groundwater flow is assumed to be essentially horizontal and is described by the groundwater flow equation for steady flow [*Bear*, 1972]:

$$\nabla^2 \phi = 0 \qquad (1)$$

where $\phi(\mathbf{x})$ is the hydraulic head [L] with respect to an arbitrary datum and $\mathbf{x} = (x, y)$ is the spatial location vector [L], where x points upstream. The specific discharge is $\mathbf{q} = -K \nabla \phi$ [LT^{-1}], the pore velocity is $\mathbf{v} = \mathbf{q}/\theta$ [LT^{-1}] where K is the hydraulic conductivity [LT^{-1}] and θ is the porosity, and the total flow integrated over the saturated aquifer thickness is $\mathbf{Q} = -Kh\nabla\phi$ [L^{2}T^{-1}]. Notice that the impermeable layer is assumed horizontal; however, the model can be easily extended to a layer with varying bottom elevation.

[9] The river, conceptualized as sinusoidal with wavelength λ [L] and amplitude α [L], has a prescribed hydraulic head $\phi_s(x) = \phi_0 + (J_x/\sigma)s(x)$, linearly varying along the river stretch, where φ_0 is the elevation of the free surface, above

the horizontal bottom, at the downstream end of the river [L], $s(x)$ is the arc length along the boundary [L] defined as

$$s(x) = \int_0^x \sqrt{1 + (2\pi\alpha/\lambda)^2 \cos^2(2\pi x/\lambda)}\,dx \qquad (2)$$

$\sigma = s(\lambda)/\lambda$ is sinuosity, and J_x is the mean head gradient along the valley in the downstream direction. The upgradient and downgradient boundaries of the domain are assumed periodic with a prescribed head drop $\phi(2\lambda, y) = \phi(0, y) + 2\lambda J_x$. Finally, the top boundary is considered a no-flow boundary and is at a distance λ from the channel axis. The resulting flow field is characterized by inflow, outflow, and no-flow zones along the domain's boundary. The assumptions about channel planimetry and boundary conditions lead to a simplified model of complex natural systems and are expected to work better when (1) the groundwater flow in the alluvial valley is preferentially parallel to the alluvial belt, (2) the river is fairly deep with uniform steady flow such that local head fluctuations, caused by riffle-pool run or other slope discontinuities, are a second-order driver of hyporheic flow and the linear head variation along the river is an acceptable

assumption, (3) there are no important preferential flow paths, e.g., paleochannels, within the point bar, and (4) the system presents minimal deep groundwater contributions. Seasonal flow dynamics determines the validity of this conceptualization, and we expect that base flow conditions result in the best approximation.

[10] In principle, Boussinesq's equation for steady flow (derived from Darcy's law and the Dupuit-Forchheimer assumption), $\nabla \cdot (\phi \nabla \phi) = 0$ is expected to produce a better solution for the flow field than equation (1), especially because small values of hydraulic gradient ($J_x^2 \ll 1$) lead to small errors with this approximation [Bear, 1972]. Notice, however, that if we express the hydraulic head ϕ as the sum of a fixed value, here we use ϕ_0, and a fluctuation ϵ (i.e., $\phi(\mathbf{x}) = \phi_0 + \epsilon(\mathbf{x})$), Boussinesq's equation can be recast for bottom elevation $z_i = 0$ as $\nabla \cdot ((\phi_0 + \epsilon) \nabla \epsilon) \approx \nabla \cdot (\phi_0 \nabla \epsilon) = \phi_0 \nabla^2 \epsilon$, for ϵ small when compared to ϕ_0. This approximation is mathematically equivalent to equation (1). For the model in hand, a characteristic value (upper limit) of this fluctuation is given by $\epsilon \sim J_x \lambda$, then the use of the linearized equation (1) is justified as long as $J_x \lambda / \phi_0 \ll 1$. Numerical simulations with $J_x = 0.01$, $\lambda = 40$ m, and $\phi_0 = 0.5$ m, a case where large differences are expected, lead to maximum relative differences of 2.5%, 20%, and 2% in hydraulic head, Darcy flux, and mean RT, respectively. These relative differences correspond to the maximum values within the domain and tend to be localized in small areas; the relative error rapidly decreases as ϕ_0 increases, and the difference in the RTDs within the domain and along the boundaries is minimal for all cases.

2.1.1. Dimensionless Equations and Metrics for Flow

[11] Let $\phi^* = \phi/(J_x\lambda)$, $\mathbf{x}^* = \mathbf{x}/\lambda$, and $\nabla(\cdot) = \nabla^*(\cdot)/\lambda$, then the mathematical statement for flow can be recast as

$$\nabla^{*2}\phi^* = 0 \tag{3a}$$

$$\phi^*(\mathbf{x}^*) = \phi_0^* + (1/\sigma)(s(x)/\lambda) \text{ for } \partial\Omega_{in} \cup \partial\Omega_{out} \tag{3b}$$

$$\mathbf{n} \cdot (-K\nabla^*\phi^*) = 0 \text{ for } \partial\Omega_{top} \tag{3c}$$

$$\phi^*(x^* = 2, y^*) = \phi^*(x^* = 0, y^*) + 2 \text{ for } \partial\Omega_{up} \text{ and } \partial\Omega_{down} \tag{3d}$$

where $\partial\Omega_{in}$ represents the sections of the river boundary with exchange from the channel to the HZ, $\partial\Omega_{out}$ represents the sections of the river boundary with exchange from the HZ to the channel, $\partial\Omega_{top}$ is the top boundary, and $\partial\Omega_{up}$ and $\partial\Omega_{down}$ are the upgradient and downgradient boundaries of the alluvial valley.

[12] Notice that ϕ_0^* is the only term in (3) that depends on J_x and therefore ϕ^* depends on both valley slope and sinuosity. The dimensionless Darcy flux

$$\mathbf{q}^*(\mathbf{x}^*) = \frac{\mathbf{q}(\mathbf{x})}{KJ_x} = -\nabla^*\phi^* \tag{4}$$

depends only on sinuosity (α and λ).

[13] Similarly, we can define a dimensionless exchange flux per unit stream length between the stream and the hyporheic zone

$$q_s^*(\mathbf{x}^*) = \frac{\mathbf{n} \cdot (-K\phi\nabla\phi)}{K\phi_0 J_x}\bigg|_{\mathbf{x}\in\partial\Omega_{out}} \approx \mathbf{n} \cdot \mathbf{q}^*(\mathbf{x}^*)\bigg|_{\mathbf{x}^*\in\partial\Omega_{out}} \tag{5}$$

where we assumed $\phi/\phi_0 \approx 1$ given the small J_x values explored. The total dimensionless exchange flux from the hyporheic zone to the stream is

$$Q^* = \frac{\int_{\partial\Omega_{out}} q_s^*(\mathbf{x}^*)\mathrm{d}\mathbf{x}^*}{s_{out}} \tag{6}$$

where $s_{out} = \int_{\partial\Omega_{out}} \mathrm{d}\mathbf{x}^*$ is the length of the channel with hyporheic flux returning to the stream. Then, $\mathbf{q}^*$, q_s^*, and Q^* depend only on α and λ, and these variables can be rescaled for a particular valley slope and hydraulic conductivity by multiplying by J_x and K, respectively.

2.2. Modeling of Residence Time Distributions

[14] For a representative elementary volume (REV) centered at a location $\mathbf{x}$ and observed at time t, the residence time distribution $\rho(\mathbf{x}, t, \tau)$ represents the proportion of particles within the REV with a RT τ ($\tau \geq 0$). In other words, the function ρ can be understood as the probability distribution function (pdf) of residence times at a given location and time. Then, the product $\rho(\mathbf{x}, t, \tau)\mathrm{d}\xi$ is the probability of finding water particles with a RT within the interval $[\xi, \xi + \mathrm{d}\xi]$ at the location $\mathbf{x}$ and time t and the integral over all residence times equals unity, i.e.,

$$\int_0^\infty \rho(\mathbf{x},t,\xi)\mathrm{d}\xi = 1. \tag{7}$$

[15] Under steady flow conditions, the RTD becomes time invariant; assuming no sources or sinks and constant porosity, the spatial evolution of ρ is described by the following partial differential equation (PDE) (see Appendix A for a derivation of the vertically integrated model and Ginn [1999] for a detailed description of the theory of RTDs):

$$\frac{\partial\rho}{\partial\tau} - \nabla \cdot (\mathbf{D}\nabla\rho) + \nabla \cdot (\mathbf{v}\rho) = 0 \tag{8}$$

where the hydrodynamic transport operator $L(\rho) = \nabla \cdot (\mathbf{D}\nabla\rho) - \nabla \cdot (\mathbf{v}\rho)$ considers Darcy's scale advection and Fickian dispersion. The average pore velocity is estimated as $\mathbf{v} = -(\theta^{-1}K\nabla\phi)$ and the dispersion-diffusion tensor $\mathbf{D} = \{D_{ij}\}$ is defined as [Bear, 1972]

$$D_{ij} = \alpha_T|\mathbf{v}|\delta_{ij} + (\alpha_L - \alpha_T)v_iv_j/|\mathbf{v}| + D_m^* \tag{9}$$

with α_T and α_L the transverse and longitudinal dispersivities, respectively, D_m^* the effective molecular diffusion coefficient, and δ_{ij} the Kronecker delta function.

[16] The cumulative residence time distribution (CRTD), or $R(\mathbf{x}, \tau)$, represents the contribution of particles younger than τ and is defined as

$$R(\mathbf{x},\tau) = \int_0^\tau \rho(\mathbf{x},\xi)\mathrm{d}\xi \tag{10}$$

The PDE that describes its evolution can be obtained by integrating equation (8). Numerically, solving for the CRTD is an easier and more stable problem, since the boundary and initial conditions are easier to handle. We model the CRTD and then estimate the RTD as $\rho(\mathbf{x}, \tau) = \partial R(\mathbf{x}, \tau)/\partial\tau$.

[17] Equation (8) is an initial value problem in the RT (τ) dimension with initial condition $\rho(\mathbf{x},\ \tau\ =\ 0)\ =\ 0$ (or $R(\mathbf{x}, \tau = 0) = 0$). Boundary conditions depend on the flow field characteristics. For instance, no-flow boundaries for flow (e.g., top of the domain) correspond to no-flux boundaries for RT, $\mathbf{n} \cdot (\mathbf{v}\rho - \mathbf{D}\nabla\rho) = 0$ (or $\mathbf{n} \cdot (\mathbf{v}R - \mathbf{D}\nabla R) = 0$), where $\mathbf{n}$ is an outward vector normal to the boundary. For outward flow (e.g., along the outflow sections of the stream boundary, $\partial\Omega_{out}$) an advective boundary condition is assumed, $\mathbf{n} \cdot \mathbf{D}\nabla\rho = 0$ (or $\mathbf{n} \cdot \mathbf{D}\nabla R = 0$), and for inward flow (e.g., along the inflow sections of the stream boundary, $\partial\Omega_{in}$) the residence time distributions is prescribed. Water recharging from the river is assumed to have a RTD concentrated at zero (new water), which is represented by a Dirac delta function $\rho(\mathbf{x}, t, \tau) = \delta(\tau)$ (a Heaviside step function for the CRTD $R(\mathbf{x}, t, \tau) = H(\tau)$). The RTD for water entering the system through the upgradient alluvial valley is unknown; however, we propose a periodic boundary condition (PBC) for RT to deal with the uncertainty associated with the alluvial valley residence time distributions and account for a cycle of upstream meanders. The PBC approach assumes that the lateral boundaries are periodic boundaries for RT, $\rho(0, y, \tau) = \rho(2\lambda, y, \tau)$, accounting for the contribution of one upstream cycle of this periodic system and neglecting contributions farther upstream, which are expected to represent a small fraction of the incoming water interacting with the HZ (see Figure 1b), or from regional groundwater flow systems.

[18] A two-wavelength domain guarantees that numerical instabilities, caused by the PBC at the lateral boundaries, are dissipated before reaching the hyporheic zone of interest and is consistent with previous works [e.g., *Cardenas*, 2009a, 2009b]. Notice, however, that the selected domain size constrains the paths followed by water molecules in the sediments and hence their residence times. This is critical for water molecules in the alluvial valley and can potentially influence the residence times within the hyporheic zone of interest. A sensitivity analysis (not shown) demonstrates that our results are independent of the domain length. We performed simulations with one- and two-wavelength domains and the flow field and RTDs are almost identical with relative differences smaller than 4% in the scenarios with higher mixing between the alluvial valley and the HZ.

[19] The CRTD, $R(\mathbf{x}, \tau)$, describes the probability of finding water particles at a location $\mathbf{x}$ with RTs lower or equal than τ, where these particles entered the system through the river. Note that for large τ, this cumulative distribution is not required to asymptotically converge to one everywhere in the domain, since we are neglecting the contribution of older waters entering the system through the lateral boundaries. Only points close to the river, where most of the water is riverine in origin, converge to one. On the other hand, points away from the river will converge asymptotically to a value lower than one, since some or all the contributions of the older waters moving through the alluvium are neglected. The difference between one and this lower value is an estimate of the proportion of older water.

[20] The complete mathematical statement used to describe the CRTD is

$$\frac{\partial R}{\partial \tau} - \nabla \cdot (\mathbf{D}\nabla R) + \nabla \cdot (\mathbf{v}R) = 0 \qquad (11a)$$

$$R(\mathbf{x},\tau) = H(\tau) \text{ inflow boundaries along the river} \left(\partial\Omega_{in}\right) \quad (11b)$$

$$\mathbf{n} \cdot (\mathbf{D}\nabla R) = 0 \text{ outflow boundary along the river} \left(\partial\Omega_{out}\right) \quad (11c)$$

$$\mathbf{n} \cdot (\mathbf{v}R - \mathbf{D}\nabla R) = 0 \text{ top boundary} \left(\partial\Omega_{top}\right) \qquad (11d)$$

$$R(0,y,\tau) = R(2\lambda,y,\tau) \text{ lateral PBC} \left(\partial\Omega_{up} \text{ and } \partial\Omega_{down}\right) \quad (11e)$$

The moments of the RTD are an important metric defined as

$$a_n(\mathbf{x}) = \int_0^\infty \xi^n \rho(\mathbf{x}, \xi)\mathrm{d}\xi \qquad (12)$$

It can be shown that for $n = 1, 2,..$ and $a_0(\mathbf{x}, t) = 1$ the complete mathematical statement for the moments is [e.g., *Varni and Carrera*, 1998; *Ginn*, 1999]

$$\nabla \cdot (\mathbf{D}\nabla a_n) - \nabla \cdot (\mathbf{v}a_n) = -na_{n-1} \qquad (13a)$$

$$a_n(\mathbf{x}) = 0 \text{ for } \partial\Omega_{in} \qquad (13b)$$

$$\mathbf{n} \cdot (\mathbf{D}\nabla a_n) = 0 \text{ for } \partial\Omega_{out} \qquad (13c)$$

$$\mathbf{n} \cdot (\mathbf{v}a_n - \mathbf{D}\nabla a_n) = 0 \text{ for } \partial\Omega_{top} \qquad (13d)$$

$$a_n(0,y) = a_n(2\lambda,y) \text{ for } \partial\Omega_{up} \text{ and } \partial\Omega_{down} \qquad (13e)$$

These moments can be related to the standard central moments with the following relationships:

$$\mu_\tau = \mathrm{E}[\tau] = a_1 \qquad (14)$$

$$\sigma_\tau = \sqrt{\mathrm{Var}[\tau]} = \sqrt{a_2 - \mu_\tau^2} \qquad (15)$$

where μ_τ and σ_τ are the mean and standard deviation of the RTD, respectively.

2.2.1. Dimensionless Equations and Metrics for Residence Time

[21] We scale RTs by the following estimate of turnover time (ratio of the HZ volume and the total exchange flux leaving the HZ):

$$T = \frac{\alpha\lambda\phi_0}{\int_{\partial\Omega_{out}} \mathbf{n} \cdot (-K\phi\nabla\phi)\mathrm{d}\mathbf{x}} \approx \frac{l_0}{KJ_x} \qquad (16)$$

where

$$l_0 = \frac{\alpha\lambda}{s_{out}Q*}$$

is a characteristic length scale independent of J_x and K. The timescale T is defined under the assumption that the planimetric area of the hyporheic zone can be approximated by $\alpha\lambda$ and $\phi/\phi_0 \approx 1$. This is a fair assumption for the parameters explored in this work.

[22] The dimensionless RT is defined as

$$\tau^* = \frac{\tau}{T} \qquad (17)$$

and the mathematical statement (11) is recast in dimensionless form by replacing τ with τ^*, $\mathbf{x}$ with $\mathbf{x}^* = \mathbf{x}/\lambda$, velocity $\mathbf{v}$ with $\mathbf{v}^* = (l_0\mathbf{q}^*)/(\theta\lambda)$, and dispersion coefficient D_{ij} with D_{ij}^* which is written in terms of the dimensionless pore velocity, $\mathbf{v}^*$, the dimensionless dispersivities, α_L/λ and α_T/λ, and by neglecting effective molecular diffusion. The resulting dimensionless mathematical statement is independent of J_x and K. Given that

$$R(\tau^*) = R\left(\frac{KJ_x}{l_0}\tau\right) \qquad (18)$$

the effect of J_x and K is to stretch or compress R and ρ in the RT domain. The sinuosity variables α and λ have a more complex impact on the shape of the RTD, because they also scale the dimensionless pore velocity ($\mathbf{v}^*$) and dispersion coefficient ($\mathbf{D}^*$). The RTD is estimated as

$$\rho(\tau) = \frac{\partial R}{\partial \tau} = \frac{KJ_x}{l_0}\frac{\partial R}{\partial \tau^*} \qquad (19)$$

For a given sinuosity and aquifer dispersivity, estimating the dimensionless CRTD, $R(\tau^*)$, allows us to explore a wide range of RTs, valley slopes, and hydraulic conductivities with a single simulation (see equation (18)). For example, the value of $R(\tau_1)$ for a given $K = K_1$, $J_x = J_{x1}$, and $\tau = \tau_1$ is obtained by evaluating the dimensionless CRTD at $\tau_1^* = (K_1 J_{x1}\tau_1)/l_0$. Moreover, if we scale any of the initial values K_1, J_{x1}, or τ_1 by a factor β, the value of R is obtained by evaluating $R(\tau^*)$ at $\tau^* = \beta\tau_1^*$. This fact is used in later sections.

[23] The dimensionless nth moment of the age distribution is defined as

$$a_n^* = \frac{a_n}{T^n} \qquad (20)$$

and the mathematical statement (13) is recast in dimensionless form with a_n^*, τ^*, $\mathbf{x}^*$, $\mathbf{v}^*$, and D_{ij}^*. As before, the resulting dimensionless mathematical statement is independent of J_x and K. Finally, expressions for the dimensionless mean and standard deviation can be expressed as

$$\mu_\tau^* = \frac{\mu_\tau}{T} = a_1^*$$
$$\sigma_\tau^* = \frac{\sigma_\tau}{T} = \sqrt{a_2^* - (\mu_\tau^*)^2}.$$

2.3. Metrics to Evaluate the Meander's Net Response

[24] The dimensionless metrics defined in previous sections are used to describe the spatial variability of fluxes and RTDs. A dimensionless framework allow us to separate the individual effect of the valley slope (J_x), hydraulic conductivity (K), and sinuosity (represented by α and λ). Furthermore, given our interest in characterizing the net response of the hyporheic zone relative to the net amount of exchange, flux-weighted distributions and central moments are estimated along the meander of interest for the water exiting the HZ. The flux-weighted and total flux-weighted values of ζ, where the scalar ζ represents either $\rho(\mathbf{x}, \tau^*)$, $R(\mathbf{x}, \tau^*)$, $\mu_\tau^*(\mathbf{x})$, or $\sigma_\tau^*(\mathbf{x})$, are defined as

$$\zeta_{FW}(\mathbf{x}, \tau^*) = \frac{(\mathbf{n}\cdot\mathbf{q})\zeta(\mathbf{x}, \tau^*)}{\int_{\partial\Omega_{out}} \mathbf{n}\cdot\mathbf{q}\,d\mathbf{x}} \qquad (21)$$

$$\zeta_{FW}^T(\tau^*) = \int_{\partial\Omega_{out}} \zeta_{FW}(\mathbf{x}, \tau^*)\,d\mathbf{x}. \qquad (22)$$

[25] To explore the flow distribution along the meander of interest (see Figure 1a), a dimensionless upstream distance $s^* = [s(x) - s(\lambda/4)] / [s(5\lambda/4) - s(\lambda/4)]$ is used. This is a standardized distance along the stream channel with respect to $s(\lambda/4)$, which means that s^* is 0 and 1 at the downstream and upstream ends of the meander, respectively.

3. Results and Discussion

[26] All simulations assume a stream meander wavelength $\lambda = 40$ m. Meander amplitude α and aquifer dispersivity α_L are explored over the intervals $\alpha/\lambda \in [1/40, 15/40]$ (sinuosity $\sigma \in [1.006, 1.866]$) and $\alpha_L/\lambda \in [1/80, 16/80]$. We assume constant porosity, hydraulic conductivity, aquifer dispersivity, and the ratio $\alpha_T/\alpha_L = 0.1$ for all cases. The finite element method implemented in COMSOL Multiphysics is used for the numerical solutions. To avoid numerical dispersion or other instabilities a fine mesh with an average element size of $\lambda/200$ (0.2m) within the HZ and $\lambda/100$ (0.4m) in the alluvial valley is used. This corresponds to about 67,000 triangular elements that produce mesh-independent solutions.

3.1. Flow

[27] The dimensionless Darcy flux normal to the stream channel (q^*_s) is shown in Figure 2a for the interval $s^* \in [0, 0.5]$. The flux is symmetric with respect to the meander apex ($s^* = 0.5$), being positive (outflow) for $s^* \in [0, 0.5]$ and negative (inflow) for $s^* \in [0.5, 1]$. The magnitude of the outward Darcy flux is zero at $s^* = 0$ and $s^* = 0.5$, reaching a maximum in between. As the meander sinuosity increases (larger α) the fluxes (q^*_s) and total exchange Q^* increase, the location of maximum outward Darcy flux moves downstream and approaches $s^* = 0$, and the along-channel distributions of flux involves a wider range of contributing flow paths. These characteristics are reflected in the total flux-weighted RTDs. For example, larger fluxes close to $s^* = 0$ lead to more important contributions of the longer flow paths, and therefore older modes in the resulting RTDs. Furthermore, as the contribution of flow paths becomes wider, the spreading of the RTD and the weight of its tail reduces, since it is integrating over flow paths with similar and equally important characteristic timescales. Exploratory simulations (not shown) demonstrate that these characteristics are persistent even for relatively small distances to the top boundary.
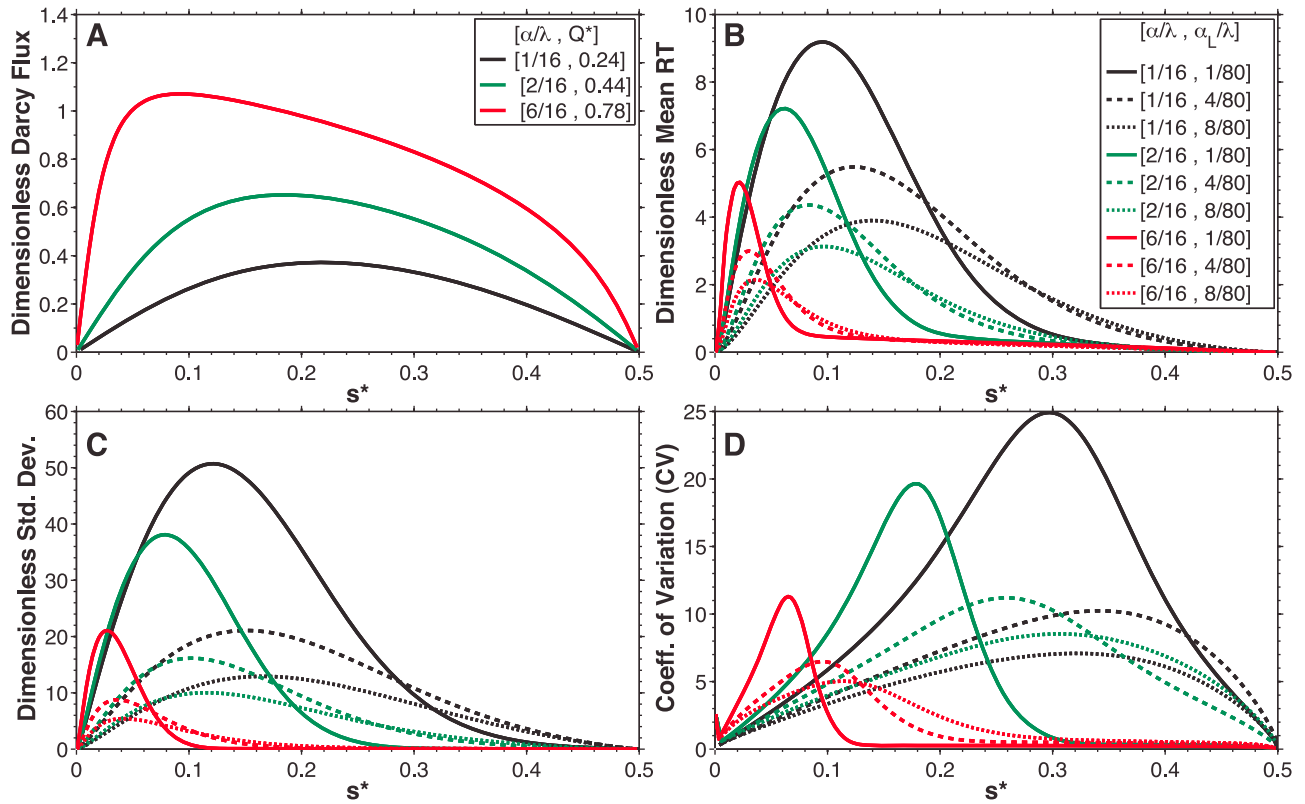
Figure 2. (a) Dimensionless Darcy flux, (b) mean RT, (c) standard deviation, and (d) coefficient of variation of dimensionless RT along the outflow boundary for the meander of interest ($s \in [s(\lambda/4), s(5\lambda/4)]$). The distance along the channel, with respect to the location $s(\lambda/4)$, is expressed in dimensionless form as $s^* = [s(x) - s(\lambda/4)]/[s(5\lambda/4) - s(\lambda/4)]$.

[28] As shown in section 2.1.1, the dimensionless Darcy flux is independent of J_x and K. However, changes in sinuosity display a nonlinear and monotonically increasing relationship with both dimensionless Darcy flux ($\mathbf{q}^*$) and total dimensionless exchange (Q^*) (see Figure 5c). *Cardenas* [2009a, equation (3)], for example, fitted a function of the form

$$Q^* \propto \frac{c_1}{\sigma} - \frac{c_2}{\sigma^2} - c_3$$

to the modeled exchange, with c_1, c_2, and c_3 positive constants. Based on our model, increases in the valley slope and hydraulic conductivity lead to a proportional increase in the hyporheic exchange. On the other hand, increases in sinuosity due to natural geomorphic processes, or anthropogenically induced during restoration practices, increase the hyporheic exchange in a nonlinear fashion. Furthermore, the rate at which exchange increases rapidly decreases with sinuosity, suggesting that increasing sinuosity for HZ restoration purposes, at least in terms of water exchange, can be optimized to the point at which increments in increases in exchange fluxes are negligible. This statement is limited to the channel geometry and assumptions of the proposed conceptual model, but are consistent with commonly found systems.

3.2. Residence Time Distributions

[29] Flow paths discharging along the stream boundary ($s^* \in [0, 0.5]$) are characterized by different RTDs. The contribution of each flow path to the resulting total flux-weighted RTD (see equation (22)), and therefore to the net response of the HZ, depends on its discharge rate. To account for this flux dependence and explore the spatial variability of the RTD metrics, flux-weighted (see equation (21)) dimensionless mean RT, standard deviation, and coefficient of variation (CV) are used.

[30] As the sinuosity increases (black, green, and red lines in Figures 2b–2d) the magnitude of the flux-weighted dimensionless moments decreases and the along-channel distribution of $\mu_{\tau,FW}^*$ and $\sigma_{\tau,FW}^*$ becomes skewed more toward the downstream end (left), leading to larger mean RT and standard deviations closer to $s^* = 0$ (Figures 2b and 2c). Moreover, the maximum for the CV curves, which is associated with flow paths that have more variable RTDs, decreases in magnitude and moves downgradient (toward $s^* = 0$) as sinuosity increases (Figure 2d). The effect of increasing dispersion (solid, dashed, and dotted lines in Figures 2b–2d) is to decrease the values of the moments and generate a more spatially uniform distribution of mean and standard deviations discharging along the channel (decrease in skewness). The spatial variability of the RTDs along the discharge section of the meander are critical to design sampling strategies and interpret experimental data aimed to quantify the biogeochemical evolution of HZ water, especially for point samples taken from piezometers or observation wells.

[31] A sensitivity analysis for the effect of sinuosity ($\alpha/\lambda \in [1/40, 15/40]$ or $\sigma \in [1.006, 1.866]$) and mixing ($\alpha_L/\lambda \in [1/80, 20/80]$) on the total flux-weighted
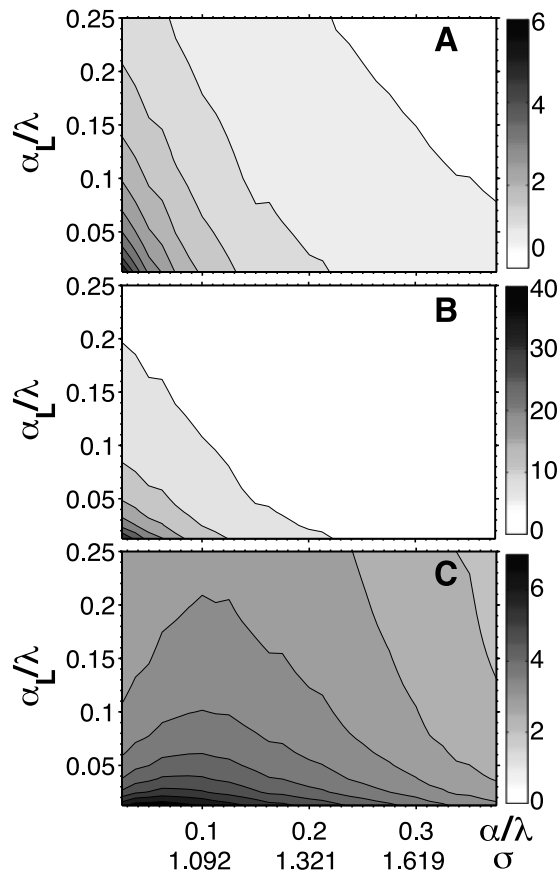
Figure 3. Sensitivity analysis for (a) the total flux-weighted (see equation (22)) dimensionless mean RT,(b) dimensionless standard deviation, and (c) coefficient of variation for water leaving the HZ, as a function of sinuosity (x axis) and mixing (represented by the dispersivity; y axis).

dimensionless mean RT, standard deviation, and coefficient of variation show that larger moments μ_τ^* and σ_τ^* correspond to the smaller sinuosities and dispersivities (see Figures 3a–3c), which at first seems counter intuitive; however, these RTDs are characterized by heavy tails with power law behavior of the form (see Figure 4)

$$\rho \propto \tau^{-\gamma} \propto (\tau^*)^{-\gamma} \quad or \quad R \propto \tau^{-\gamma+1} \propto (\tau^*)^{-\gamma+1} \quad (23)$$

where the coefficient γ increases with sinuosity and aquifer dispersivity (see Figure 5b), leading to smaller contributions of long residence times (lighter tails) and biasing the mean and standard deviation toward smaller values. The spreading of these distributions is evidenced by the large values of CV (CV > 1) over the range of variables explored (see CV surface in Figure 3c). This behavior of the central moments is indicative of the large uncertainty in their use to characterize biogeochemical reactions in the HZ [e.g., *Hoehn and Cirpka*, 2006; *Lamontagne and Cook*, 2007; *Jiang et al.*, 2010; *Marzadri et al.*, 2010].

[32] For the system in hand, the contribution of the first mode of the distribution τ_{CTS} (or τ_{CTS}^* in dimensionless terms) and the exponent of the power law region are better descriptors of how sinuosity and dispersion influence RTDs. For instance, a considerable amount of the contribution arrives at τ_{CTS}^*, which means that this timescale characterizes the dominant biogeochemical processes that affect the HZ water discharging to the stream. On the other hand, the exponent γ characterizes the more persistent and long-term contributions to the stream.

[33] The main mode of the RTD, τ_{CTS}^*, is associated with the dominant advective transport paths and is the characteristic timescale for the dominant contributions from the HZ to the stream. This timescale increases with sinuosity, until it reaches a plateau, and decreases with dispersion (Figure 5a). For small dispersion ($\alpha_L/\lambda = 1/80$ and $2/80$) the plateau is reached around $\alpha/\lambda = 0.1$ ($\sigma = 1.092$), corresponding to a moderate value of γ, which is ideal from the point of view of allowing longer times for biogeochemical evolution in low-sinuosity channels.

[34] The magnitude of the exponent γ increases with sinuosity until it reaches a plateau (Figure 5b). As dispersion increases, the exponent and the sinuosity needed to reach the plateau also increase. These trends imply a more important contribution of the RTD's tail for smaller sinuosities and dispersivities, with a more persistent contribution of the HZ to the stream involving the long-term release of older and more biogeochemically evolved waters. Additionally, the range of RTs over which this power law behavior is observed, before the onset of exponential decay, decreases as sinuosity or dispersivity increase.

[35] Previous modeling efforts found a similar functional form for the meander RTDs [*Cardenas*, 2008a, 2008b;
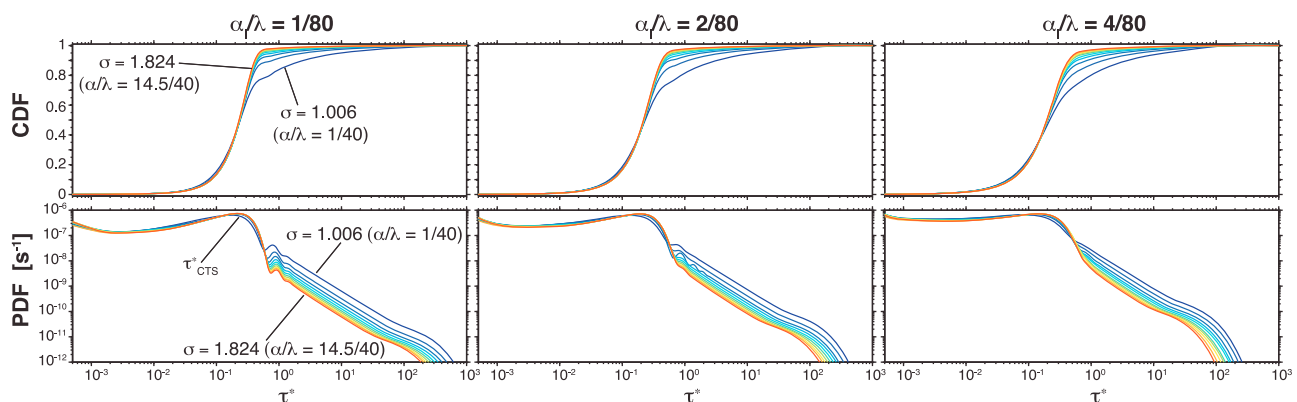
Figure 4. Total flux-weighted (top) CRTD and (bottom) RTD in the exchange discharge. Colors represent different sinuosities and different dispersivities, α/λ, are shown. Dimensionless time τ^* is used and the RTDs corresponds to $J_x = 0.002$ and $K = 10^{-3}$ m/s.
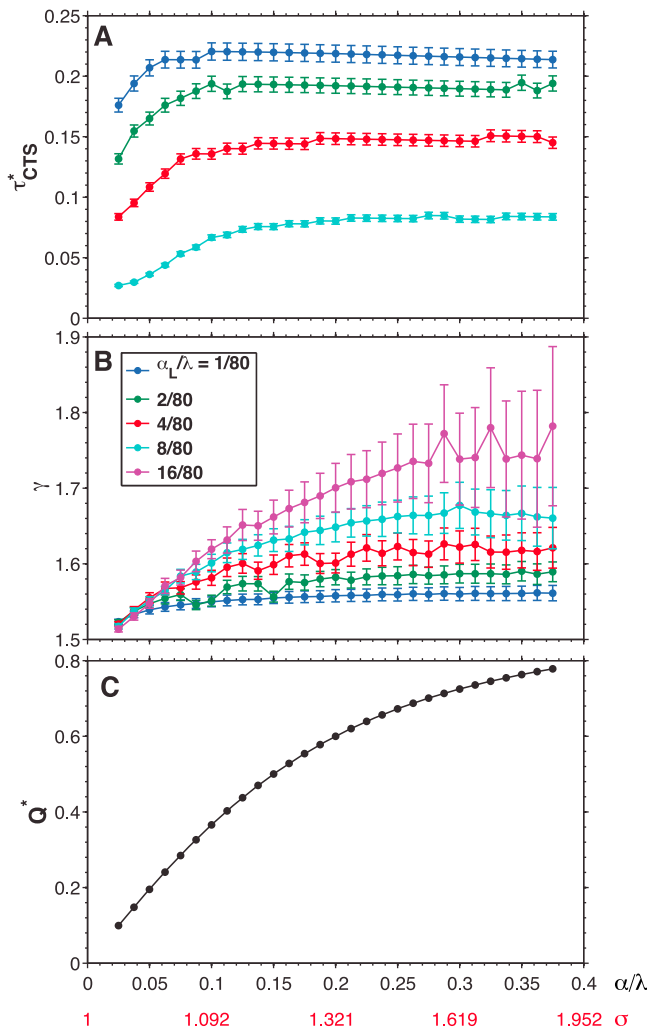
Figure 5. Results of the sensitivity analyses for the total flux-weighted RTDs. (a) Dimensionless characteristic timescale, τ^*_{CTS}, and (b) power law exponent, γ, as a function of sinuosity for several mixing scenarios. Error bars correspond to the 95% confidence interval, and fluctuations are caused by outliers included during the selection of the interval with power law behavior. (c) Total dimensionless hyporheic exchange as a function of sinuosity.
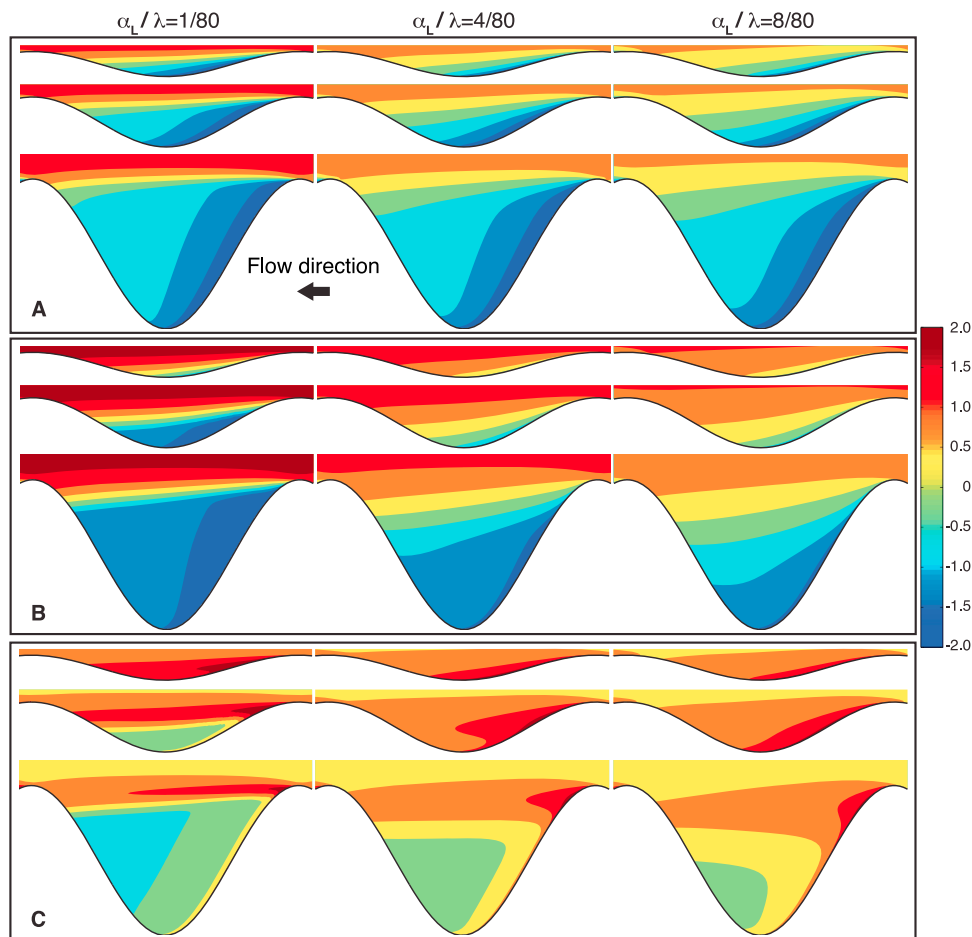
transport characterized by power law residence time distributions. This has important implications for the transport, retention, and transformation of solutes at the watershed scale, especially as it gives evidence of the long-term influence of the hyporheic exchange. The power law behavior observed in this study is similar to the one observed by *Revelli et al.* [2008] and *Cardenas* [2008a, 2008b]; however, the planimetry used in these previous works is characterized by larger sinuosities with a narrow meander neck, which leads to power law behavior in between the peaks corresponding to the characteristic timescales for the meander neck and core. Our simulations result in multimodal distributions for small values of dispersivity, but these modes, associated with older waters in the alluvium, are smoothed out as the mixing increases (see Figure 4).

[36] Recall that the net contribution of the HZ to the stream biogeochemistry is a function of both RT and exchange flux. Even though small sinuosities present heavier tails in the total flux-weighted RTDs, and therefore more persistent and larger proportions of biogeochemically evolved water, the overall contribution is small, given the limited amount of exchange (see Figure 5c). On the other hand, as sinuosity increases the amount of exchange and τ^*_{CTS} increase, leading to a more efficient reactor. In this case, it is critical to compare the RTD to the characteristic timescales for the biogeochemical transformations of interest. This topic is explored in section 3.3.

[37] Spatial patterns for $\log_{10}(\mu^*_\tau)$, $\log_{10}(\sigma^*_\tau)$, and $\log_{10}(CV)$ are shown in Figures 6a–6c, respectively. Different values of dispersivity and sinuosity are show in Figure 6. Notice that these moments are scaled by J_x and K, so a twofold increase in J_x or K leads to a half decrease in the moment. The patterns and magnitude of CV are independent of J_x and K. The moments change over 3 orders of magnitude for $\alpha_L/\lambda = 1/80$ and 2 orders of magnitude for $\alpha_L/\lambda = 4/80$ and $\alpha_L/\lambda = 8/80$. As dispersivity increases, the contribution of older waters, from the alluvial valley, to the hyporheic zone increases. This is expected, since mixing increases the opportunity for interaction of the HZ with groundwater traveling along the alluvial valley. Notice that the variability of the RTD, as measured by the CV, within the HZ increases with increasing dispersion and decreasing sinuosity (Figure 6c). In other words, increases in sinuosity lead to less variable and more concentrated spatial distribution of RTDs.

3.3. Biogeochemical Effects: An Application Example

[38] To relate the flow timescales represented by the RTDs and their impacts on the biogeochemical evolution of sinuosity-driven hyporheic zones, we use the concept of biogeochemical timescales (BTSs) proposed by *Boano et al.* [2010a] in conjunction with the modeled RTDs to generate biogeochemical zonation patterns, evaluate the level of biogeochemical efficiency of several meanders, and quantify the role of longer flow paths. *Boano et al.* [2010b] proposed simple expressions for threshold timescales that separate the occurrence of some biologically mediated redox reactions involved in the evolution of dissolved organic carbon (DOC). As water travels through the hyporheic zone, these sequence of hierarchical reactions diminish the amount of DOC and the electron acceptors involved in its decomposition (e.g., O_2, NO_3^-, SO_4^{2-}). These timescales are used to illustrate the importance of RTDs and evaluate biogeochemical implications in a standardized manner; however, there are important

Boano et al., 2010a]. This article elaborates on this topic by focusing on the role of valley slope, hydraulic conductivity, and channel sinuosity on RTDs. *Boano et al.* [2006] explored the intrameander flux induced by river sinuosity using the meander geometry predicted by a morphodynamic model. This study showed the importance of river planimetry on the hyporheic exchange, particularly on the flow pattern and magnitude of exchange. As a continuation of this work, *Revelli et al.* [2008] used the same planimetric model and a particle tracking approach to explore both the flow patterns and the resulting RTDs. In this case, they found bimodal RTDs with intermediate power law behavior, which is explained by a zonation that separates slow fluxes and low discharges in the core of the meander from fast and intense exchange in the meander's neck. *Cardenas* [2008b] used a planimetric morphology similar to the one used by *Boano et al.* [2006] to show that sinuosity-driven hyporheic exchange in homogeneous point bars leads to non-Fickian

Figure 6. Spatial patterns of logarithm of (a) dimensionless mean RT, (b) standard deviation, and (c) coefficient of variation of dimensionless RT. Rows correspond to different sinuosities ($\sigma = 1.038$, 1.400, and 1.866) and different dispersivities are shown ($\alpha_L/\lambda = 1/80$, 4/80, and 8/80).

assumptions behind these expressions. For example, heterogeneity in hydraulic and chemical properties and biota, as represented by the kinetic reaction rates and other model parameters used by *Boano et al.* [2010b], is ignored. This assumption impacts the overall mobility, species configuration, and transformations within the subsurface [*Tompson and Jackson*, 1996]. Even under ideal hydraulic and chemically homogeneous conditions, the spatial distribution of active biological communities plays a fundamental role and can potentially invalidate this simplified model. In spite of these caveats, our aim in this section is to illustrate the potential of using RTDs to evaluate the biogeochemical capacity of sinuosity-driven hyporheic zones under the assumption that such biogeochemical thresholds can be found. Recent findings [e.g., *Gu et al.*, 2007; *Pinay et al.*, 2009; *Zarnetske et al.*, 2011a] suggest that this is possible in some cases, but more research is needed to constrain the range of applicability of this simple model.

[39] *Boano et al.* [2010b] defined threshold or biogeochemical timescales (t_i, $i = 1,.., n$) that correspond to the time needed for an e-fold decrease in the original stream concentration of the solute i within the hyporheic zone. The complementary cumulative RTD evaluated at t_i, $1 - R(t_i)$, defines the proportion of water molecules within a representative elementary volume that cross such a threshold, and therefore can be used to estimate the probability of having

concentrations lower than e^{-1} times the original stream concentration. For simplicity, we refer to this probability as the *probability of consumption*. In formal mathematical terms, the probability of water having a RT τ larger than a biogeochemical timescale (t_i, $i = 1,.., n$) is given by the RTD at any location in the domain as $P_i = P(\tau > t_i) = 1 - R(t_i)$, where t_i is the BTS for DOC or an electron acceptor (O_2, NO_3^-, SO_4^{2-}).

[40] For this example, we use the biogeochemical timescales for O_2, NO_3, and DOC estimated by applying the criterion of *Boano et al.* [2010b] to the data of *Zarnetske et al.* [2011a, Figures 5 and 7]. In this case, $t_{O_2} = 0.20$ d, $t_{NO_3} = 0.92$ d, and $t_{DOC} = 2.10$ d. The timescale for nitrate is similar to the ones found by *Pinay et al.* [2009], where $t_{NO_3} = 0.07$ and 0.24 d. Notice, however, that these BTSs are site dependent and can vary over a wide range of values. For instance, the kinetic reaction rate for DOC, which varies over 9 orders of magnitude ($k_{DOC} \in [10^{-7}, 10^3]$ yr^{-1}) [*Hunter et al.*, 1998], is the dominant parameter in the analytical model for BTSs proposed by *Boano et al.* [2010b], Equations (22)–(26). A sensitivity analysis, using parameter values reported in the literature [*Albarède*, 1996; *Drever*, 1997; *Langmuir*, 1997; *Hunter et al.*, 1998; *Chapelle*, 2000; *Zheng and Bennett*, 2002; *Bethke*, 2008], shows that the BTSs for oxygen and nitrate vary over 9 orders of magnitude as well (10^{-2}–10^6 d).
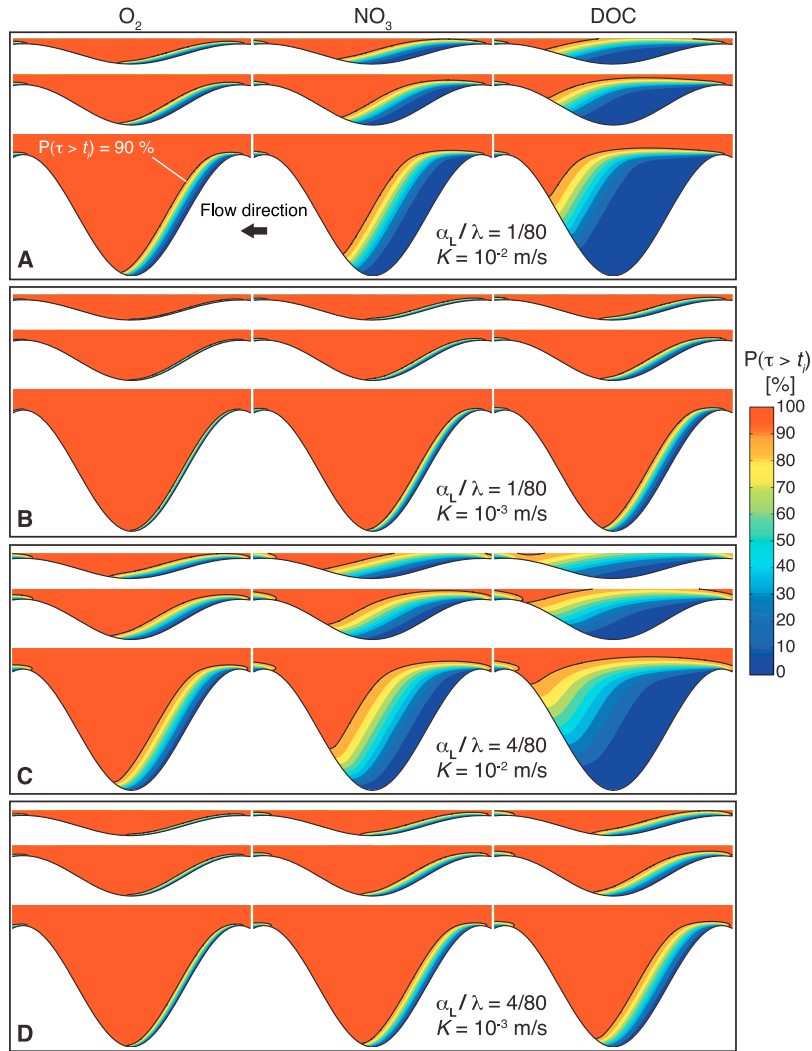
Figure 7. Probability of consumption for O_2, NO_3^-, and DOC, using the biogeochemical timescales of *Zarnetske et al.* [2011a]. Combinations of aquifer dispersivity ($\alpha_L/\lambda = 1/80$ and $4/80$) and hydraulic conductivity ($K = 10^{-3}$ and 10^{-2} m/s) are shown. Rows correspond to the different sinuosities ($\sigma = 1.038$, 1.400, and 1.866). $J_x = 0.002$ in all cases.

[41] Recall that the idea is not to explore the details of the biogeochemical modeling, but rather to map the patterns and net meander response obtained with the estimated RTDs, as a metric for biogeochemical zonation. For a given aquifer dispersivity and sinuosity, we estimate the dimensionless CRTD, $R(\tau^*)$. The probability of consumption for a solute i is then estimated as

$$P_i = P(\tau > t_i) = 1 - R\left(\tau^*_{BTS,i}\right) \qquad (24)$$

where

$$\tau^*_{BTS,i} = \frac{K J_x t_i}{l_0} = \frac{\eta_i}{l_0} \qquad (25)$$

is the dimensionless biogeochemical timescale for solute i. Then, changes in the product $\eta_i = K J_x t_i$ are related to either changes in hydraulic conductivity, valley slope, or BTS. In particular, large variability in η_i is associated to K and t_i, since these parameters can vary over several orders of magnitude. To summarize, for a given $R(\tau^*)$, we explore a range of values η_i to quantify the effect of K, J_x, or t_i on the biogeochemical potential of the meander HZ.

3.3.1. Spatial Biogeochemical Zonation

[42] The biogeochemical zonation obtained with the timescales described above is shown in Figure 7. The color scale corresponds to the probability of consumption (P_i) for oxygen, nitrate, and DOC (from left to right) and for different sinuosities, aquifer dispersivities, and hydraulic conductivities. Oxygen is readily consumed, and the anoxic and denitrification zones within the HZ increase with decreasing aquifer dispersivity (compare the zones with high probability of consumption in Figures 7a and 7c or Figures 7b and 7d) or hydraulic conductivity (compare the zones with high probability of consumption in Figures 7a and 7b or Figures 7c and 7d). Recall that the differences in the patterns obtained by decreasing the hydraulic conductivity by an order of magnitude (Figures 7a and 7b or Figures 7c and 7d), while the other parameters are held constant, are the same than the ones obtained by scaling the valley slope or the BTS by the same factor, while the other parameters are held constant. Therefore, decreases in either J_x and t_i are associated to increases in
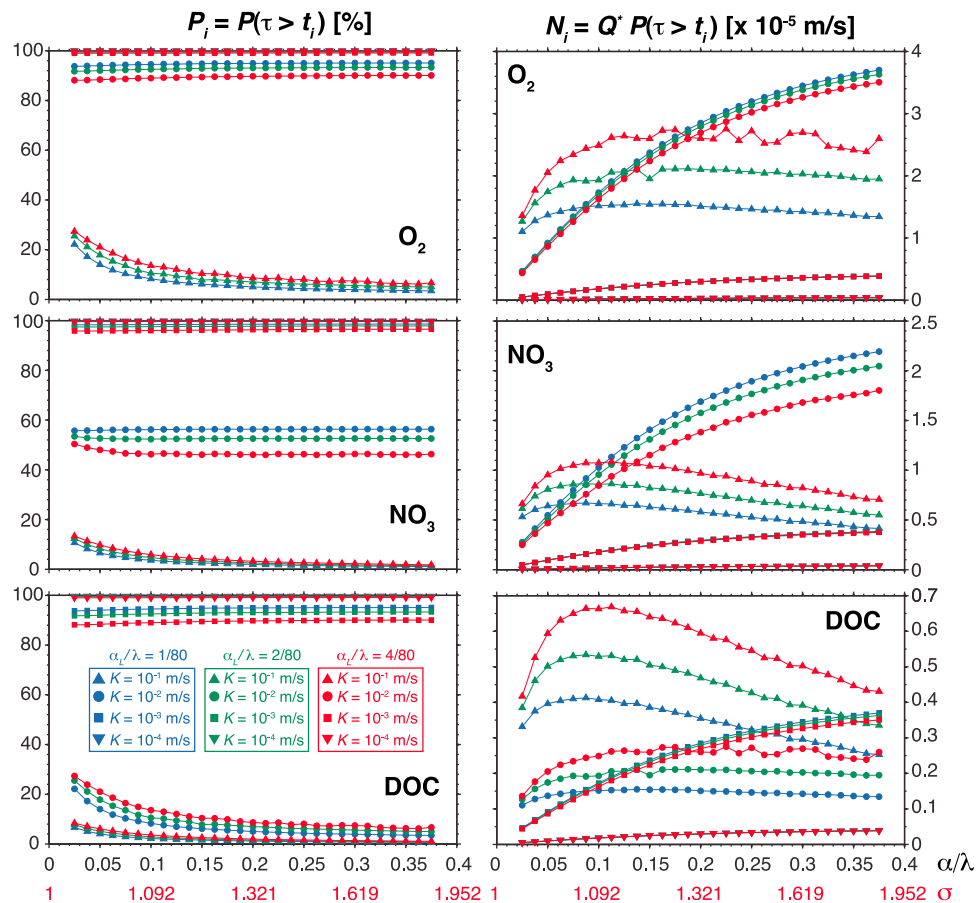
Figure 8. Probability of (left) consumption ($P(\tau > t_i)$) and (right) proportion of flux depleted of solute ($KJ_xQ * P(\tau > t_i)$) as a function of sinuosity for several aquifer dispersivities and hydraulic conductivities. The biogeochemical timescales of *Zarnetske et al.* [2011a] are used. Rows correspond to O_2, NO_3^-, and DOC. $J_x = 0.002$ in all cases.

the anoxic and denitrification zones. Large values of J_x, K, or t_i result in waters that do not have enough time to react and resurface with a biogeochemical signature that resembles the original stream water quality. As mentioned before, K and t_i can change over several orders of magnitude, playing a dominant role in the biogeochemical zonation of the HZ.

3.3.2.   Net Biogeochemical Response

[43]   The total flux-weighted RTD is used to evaluate the net biogeochemical potential of the hyporheic zone. The probability of consumption ($P_i = P(\tau > t_i)$) is a measure of the efficiency of the hyporheic zone to transform a given solute. To account for the amount of exchange, we use the product of this probability of consumption and the total exchange ($N_i = J_x KQ * P(\tau > t_i)$), which is a measure of the amount of exchange water that is depleted of a given solute before leaving the HZ. Larger values of the metrics P_i and N_i correspond to more biogeochemically efficient HZs.

[44]   For a given aquifer dispersivity, changes in hydraulic conductivity have a strong effect on the net probability of consumption (Figure 8, left). Low values of hydraulic conductivity ($K = 10^{-4}$ and $K = 10^{-3}$ m/s) are characterized by systems with high probability of consumption, leading to full consumption of oxygen, nitrate, and DOC over the range of sinuosities explored. In general, systems with low values of hydraulic conductivity are sinks of nitrate. As the value of K increases ($K = 10^{-2}$ and $K = 10^{-1}$ m/s), the behavior of

the system changes dramatically, leading to meander HZs with appreciable concentrations of nitrate in the water discharging to the stream. As explained before, similar conclusions are obtained for changes in J_x or t_i, when the other variables are held constant.

[45]   Aquifer dispersivity, on the other hand, plays a minor role in the net biogeochemical potential of the HZ (blue, green, and red lines in Figure 8, left). Increases in dispersivity can either increase or decrease the probability of consumption, depending on the solute and biogeochemical timescale. However, these changes do not influence the decision of whether or not the HZ is a net source of oxygenated waters and nitrates. Similarly, sinuosity changes have a minor effect from the point of view of the probability of consumption metric.

[46]   New patterns emerge when we account for the amount of exchange (Figure 8, right). For instance, high values of hydraulic conductivity ($K = 10^{-1}$ m/s) have an optimum sinuosity, where N_i is maximum, which varies slightly with aquifer dispersivity and solute. A meander with this optimal sinuosity discharges the largest amount of water depleted of solutes to the stream, and therefore it is the more biogeochemically efficient meander (it transforms a large amount of solutes). For example, a meander with this sinuosity is an optimal sink for nitrate, since it transforms large amounts of this nutrient and releases considerable amounts of nitrate-free

water to the stream. This behavior is expected, since the dimensionless biogeochemical timescale, $\tau^*_{BTS,i}$, associated with these scenarios is within the power law domain of the RTDs (see Figures 4 and 5b). Also, for large values of hydraulic conductivity, the efficiency of the HZ, represented by larger values of N_i, increases with decreasing aquifer dispersivity (blue, green, and red lines in Figure 8, right); however, these changes are relatively small. As the hydraulic conductivity decreases ($K = 10^{-2}$, 10^{-3} and $K = 10^{-4}$ m/s), N_i monotonically increases, mimicking a scaled version of Q^* (see Figure 5c). In this case, the effect of aquifer dispersivity is minimal, especially for low values of K.

[47] These results evidence the complex interplay between RTD's shape and the values of the threshold timescales that characterize biogeochemical transformations.

4. Conclusions

[48] In this article we explored the role of valley slope, hydraulic conductivity, and sinuosity on the residence time distributions (RTDs) for a generalized meander hyporheic zone (HZ). The use of dimensionless expressions simplifies the exploration of the parameter space, since the fluxes and the RTD and its moments can be easily scaled to account for a given value of K or J_x. Notice, however, that some of these variables can be correlated, for example, valley slope is correlated to sinuosity [*Schumm and Khan*, 1971; *Schumm*, 1985; *van den Berg*, 1995] and hydraulic conductivity [*Buffington and Tonina*, 2009]. In our simulations, we explored the range $\sigma \in [1.006, 1.865]$, which covers most natural conditions [*Cardenas*, 2009a]. To explore combinations of these sinuosities with different values of K and J_x, a simple linear scaling can be used to obtain fluxes and RTDs, leading to a broad range of scenarios in the parameter space. The examples used to evaluate the biogeochemical effects of the HZ are not exhaustive and were selected to be consistent with *Zarnetske et al.* [2011a], but the same methodology can be applied to different parameter combinations. Patterns in residence time (RT) are linked to hyporheic flow to gather the following general conclusions:

[49] 1. Total flux-weighted RTDs are characterized by one main mode, τ^*_{CTS}, and a late time power law behavior, $\rho \propto \tau^{-\gamma}$. This functional form of the RTD implies that central moments are poor descriptors of the contact times in the HZ.

[50] 2. The characteristic timescale, τ_{CTS} or τ^*_{CTS} in dimensionless terms, is associated to the main mode of the RTD and represents the dominant timescale for water leaving the HZ and discharging to the stream. It is proportional to valley slope (J_x) and hydraulic conductivity (K) and varies in a nonlinear fashion with sinuosity and aquifer dispersivity. As sinuosity increases, both τ_{CTS} and τ^*_{CTS} increase to a plateau. Also, decreases in aquifer dispersivity are associated with increases in τ_{CTS} and τ^*_{CTS}.

[51] 3. The exponent of the power law, γ, is insensitive to J_x, but increases with sinuosity and aquifer dispersivity to a plateau. This means that less sinuous channels present heavier tails in the RTD. Notice, however, that water characterized by these long RTs represent a small fraction of the total hyporheic exchange.

[52] 4. The RTD and its dependence on hydraulic conductivity, aquifer dispersivity, valley slope, and sinuosity is used to evaluate the plausible biogeochemical transformations

taking place in meander hyporheic zones. For a given solute's biogeochemical timescale, the RTD is used to evaluate whether the solute is considerably transformed during hyporheic exchange. An important application of this concept is the classification of meanders as net sinks of nitrates or only modulators of the residence times in the subsurface where nitrate reduction is negligible. The illustrative example presented in section 3.3 shows that the dominant variables in this classification are valley slope (J_x), sinuosity (σ), hydraulic conductivity (K), and biogeochemical timescale (t_i). Dispersivity plays a minor role in this classification. The physical parameters (J_x, σ, and K) can be extracted from remote sensing information such as soil maps, digital elevation models and river networks. In particular, resent work by *Luo and Pederson* [2012] demonstrated the potential of remote sensing data and GIS processing techniques to estimate K at the watershed scale based on geomorphic properties. Moreover, estimates of the biogeochemical timescales can be obtained with limited chemical data and a conceptual model such as the one proposed by *Boano et al.* [2010a].

[53] This simple conceptual model can be used to predict the net biogeochemical response and spatial patterns of flow, solute concentrations, and residence times in sinuosity-driven hyporheic zones along the river corridor at the watershed scale and from a minimum amount of information. Observations in natural systems and laboratory experiments are required to validate the model and test its robustness and limitations. Making these observations is out of the scope of this article and will be part of future research, which is fundamental to estimate the uncertainty associated with this model at the watershed scale. Experimental setups from new and previous observational studies can be used to test our theoretically predicted flow and biochemical patterns [e.g., *Wroblicky et al.*, 1998; *Baker et al.*, 1999; *Kasahara and Wondzell*, 2003; *Hoehn and Cirpka*, 2006; *Peyrard et al.*, 2008; *Pinay et al.*, 2009; *Wondzell et al.*, 2009; *Zarnetske et al.*, 2011a, 2011b; *Schneider et al.*, 2011]. In particular, new studies should be designed to explore the model consistency when the assumptions about channel pattern, heterogeneity, and groundwater flow in the alluvial valley are either met or fail. In both cases, observations can test the limits of applicability and robustness of the model in natural systems. For example, the assumption of parallel flow in the alluvial valley without contributions from longer flow paths (e.g., regional groundwater inputs) is likely dependent on seasonal dynamics at the watershed scale and can be violated at certain times during the year. Similarly, hydrologic systems where heterogeneity cannot be ignored, for example meanders with important transport along paleochannels, can potentially invalidate our results. Interestingly, dispersivity, which captures the role of advective transport due to unresolved heterogeneities, plays a minor role in the classification proposed, indicating that the model may be robust enough to overcome this issue, provided the scale of heterogeneities are small enough, but validation of this statement is necessary. Finally, field and laboratory validation of the model proposed by *Boano et al.* [2010a] for the biogeochemical timescales is required.

[54] As an illustrative example, we compare our model with observations made in three streams with contrasting parent lithology and located in western and north central New

Table 1. Summary of the Alluvial Characteristics at the NM Study Sites and Their Measured Nitrate Consumption (Measured as Uptake Length), Lateral Exchange, and Storage Zone Residence Time[a]

Site	σ (α/λ)	J_x	$K \times 10^{-5}$ (m/s)	Nitrate Uptake Length (m)	Lateral Inflow (l/s)	Storage Zone RT (min)	Q^*	N_{NO_3}
Aspen Creek	1.3 (0.193)	0.020	0.13	1778	0.396	33	0.6	0.025
Rio Calaveras	1.2 (0.153)	0.013	1.20	782	0.260	28	0.5	0.030
Gallina Creek	1.4 (0.25)	0.110	4.00	205	0.760	1257	0.7	0.3500

[a]From *Valett et al.* [1996, 1997], *Morrice et al.* [1997], *Wroblicky et al.* [1998], *Baker et al.* [1999], and *Morrice et al.* [2000]. Q^* and N_{NO_3} correspond to the total dimensionless hyporheic exchange and the proportion of flux depleted of nitrate, respectively, estimated with the proposed conceptual model, the measured hydraulic characteristics, and the biogeochemical timescales from *Zarnetske et al.* [2011a].

Mexico: Aspen Creek, Rio Calaveras, and Gallina Creek. Hereafter referred to as the New Mexico (NM) study. This comparison is mostly qualitative, since the New Mexico study focused on the interpretation of transient storage models and it is hard to separate the individual role of all the mechanisms driving hyporheic exchange and the scales at which biogeochemical transformations occur. Based on the long duration of their tracer tests and modeling exercise, we assume that lateral exchange is a first-order control in such transformations. Groundwater-surface water interactions and their role on nitrate utilization and biogeochemical evolution were observed in these alluvial systems and the findings were summarized in the seminal papers by *Valett et al.* [1996, 1997], *Morrice et al.* [1997], *Wroblicky et al.* [1998], *Baker et al.* [1999], and *Morrice et al.* [2000]. These studies focused on the role of hydraulic conductivity as a dominant factor in hydrologic retention (increase in residence times). In general, our simulations are consistent with their findings; however, the proposed conceptual model opens the possibility of having systems with similar hydraulic characteristics but a completely different net biogeochemical response, emphasizing the role of other variables such as valley slope and sinuosity.

[55] Based on the NM study observations, systems with higher alluvial hydraulic conductivity have a larger extent of surface-hyporheic interaction and retain more biologically important solutes [*Valett et al.*, 1996]. Using in-stream and well observations and a transient storage model, the New Mexico study found that as hydraulic conductivity increases the nutrient retention increases (i.e., nitrate uptake length decreases). In our case, N_i is analogous to their measure of nutrient retention. Moreover, they concluded that systems with low K consume water's dissolve oxygen as it enters the HZ and present a steep redox gradient in close proximity to the stream surface. These patterns are associated with the increase in RT and are consistent with our model (see Figure 7). Assuming that these systems have the biogeochemical timescales used by *Zarnetske et al.* [2011a], we find that retention considerably increases with K (see Table 1), consistent with the New Mexico study. Also, the characteristic timescale τ_{CTS}^* is similar in all systems over the dispersivities explored, which is consistent with the field observations, and the coefficient γ is invariant for small dispersivities ($\alpha_L/\lambda = 1/80, 2/80$) but considerably larger for large values ($\alpha_L/\lambda = 4/80, 8/80, 16/80$) (see Figures 5a and 5b). Notice, however, that according to our model, this is not only a function of the alluvial conductivity but depends on the valley slope and biogeochemical timescales (see Figure 8). There are cases with the same K and J_x values observed in the NM study that can lead to opposite behavior.

Confirmation of this requires new observations in different systems or during different hydrologic regimes.

Appendix A: Derivation of the Vertically Integrated RTD Mathematical Model

[56] The continuity equation for water molecules in a control volume centered in **x** for a vertically integrated aquifer with uniform depth is

$$\frac{\mathrm{d}}{\mathrm{d}t}(\theta\rho\phi) = \nabla \cdot [\phi(\theta\mathbf{D}\nabla\rho - \theta\mathbf{v}\rho)] \tag{A1}$$

where the left-hand side term corresponds to the time rate change of the mass in the control volume. Since ρ is a function of both t and τ, this term can be rewritten as

$$\frac{\mathrm{d}}{\mathrm{d}t}(\theta\rho\phi) = \theta\rho\frac{\mathrm{d}\phi}{\mathrm{d}t} + \phi\frac{\mathrm{d}(\theta\rho)}{\mathrm{d}t} = \theta\rho\frac{\partial\phi}{\partial t} + \phi\left(\frac{\mathrm{d}t}{\mathrm{d}t}\frac{\partial(\theta\rho)}{\partial t} + \frac{\mathrm{d}\tau}{\mathrm{d}t}\frac{\partial(\theta\rho)}{\partial\tau}\right) \tag{A2}$$

After inserting equation (A2) into equation (A1), expanding, and recalling that RT and time change at the same rate ($\mathrm{d}\tau/\mathrm{d}t = 1$), we obtain

$$\frac{\partial(\theta\rho)}{\partial t} + \frac{\partial(\theta\rho)}{\partial\tau} - \nabla \cdot (\theta\mathbf{D}\nabla\rho - \theta\mathbf{v}\rho)$$
$$= -\theta\rho\left[\frac{1}{\phi}\frac{\partial\phi}{\partial t} + \left(\mathbf{v} - \mathbf{D}\frac{\nabla\rho}{\rho}\right) \cdot \frac{\nabla\phi}{\phi}\right]. \tag{A3}$$

[57] The right-hand side of equation (A3) can be neglected for steady flow and small changes in water table (Boussinesq assumption)

$$\frac{1}{\phi}\frac{\partial\phi}{\partial t} \to 0 \quad \text{and} \quad \frac{\nabla\phi}{\phi} \to 0$$

then, the PDE describing the evolution of the RTD is

$$\frac{\partial(\theta\rho)}{\partial t} + \frac{\partial(\theta\rho)}{\partial\tau} = \nabla \cdot (\theta\mathbf{D}\nabla\rho - \theta\mathbf{v}\rho) \tag{A4}$$

Furthermore, under steady flow conditions, this equation simplifies to

$$\frac{\partial(\theta\rho)}{\partial\tau} = \nabla \cdot (\theta\mathbf{D}\nabla\rho - \theta\mathbf{v}\rho). \tag{A5}$$

Notation

ϕ hydraulic head [L].
ϕ^* dimensionless hydraulic head.
$\mathbf{x} = (x, y)$ spatial location vector [L].

$\mathbf{x}^* = (x^*, y^*)$ dimensionless spatial location vector.

$\mathbf{q}$ Darcy flux $[\mathrm{LT}^{-1}]$.

$\mathbf{q}^*$ dimensionless Darcy flux.

$\mathbf{v}$ pore velocity $[\mathrm{LT}^{-1}]$.

$\mathbf{v}^*$ dimensionless pore velocity.

q_s^* dimensionless exchange flux per unit stream length between the stream and the hyporheic zone.

Q total flow integrated over the saturated aquifer thickness $[\mathrm{L}^2\mathrm{T}^{-1}]$.

Q^* total dimensionless exchange flux from the hyporheic zone to the stream.

K hydraulic conductivity $[\mathrm{LT}^{-1}]$.

θ porosity.

λ, α wavelength $[\mathrm{L}]$ and amplitude $[\mathrm{L}]$ of the sinusoidal river.

θ porosity.

ϕ_s hydraulic head prescribed along the river stretch $[\mathrm{L}]$.

ϕ_0 elevation of the free surface at the downstream end of the river $[\mathrm{L}]$.

s arc length along the river boundary $[\mathrm{L}]$.

σ river sinuosity.

J_x mean head gradient along the valley in the downstream direction.

s_{out} length of the channel with hyporheic flux returning to the stream $[\mathrm{L}]$.

t time $[\mathrm{T}]$.

τ residence time $[\mathrm{T}]$.

τ^* dimensionless residence time.

ρ residence time distribution RTD $[\mathrm{T}^{-1}]$.

R cumulative residence time distribution CRTD.

$\mathbf{D} = \{D_{i,j}\}$ dispersion-diffusion tensor $[\mathrm{L}^2\mathrm{T}^{-1}]$.

$\mathbf{D}^* = \{D_{i,j}^*\}$ dimensionless dispersion-diffusion tensor.

D_m^* effective molecular diffusion coefficient $[\mathrm{L}^2\mathrm{T}^{-1}]$.

α_T, α_L transverse and longitudinal dispersivities $[\mathrm{L}]$.

α_T^*, α_L^* dimensionless transverse and longitudinal dispersivities.

$\delta_{i,j}$ Kronecker delta function.

$\delta(\tau), H(\tau)$ Dirac delta $[\mathrm{T}^{-1}]$ and Heaviside step functions evaluated in the residence time τ.

a_n nth moment of the RTD $[\mathrm{T}^n]$.

a_n^* dimensionless nth moment of the RTD.

μ_τ, σ_τ mean $[\mathrm{T}]$ and standard deviation $[\mathrm{T}]$ of the RTD.

$\mu_\tau^*, \sigma_\tau^*$ dimensionless mean and standard deviation of the RTD.

s^* dimensionless upstream distance.

T turnover time $[\mathrm{T}]$.

l_0 characteristic length scale $[\mathrm{L}]$.

τ_{CTS} first mode of the RTD $[\mathrm{T}]$.

τ_{CTS}^* dimensionless first mode of the RTD.

γ exponent of the power law region of the RTD.

t_i biogeochemical timescale for the solute i $[\mathrm{T}]$.

$\tau_{BTS,i}^*$ dimensionless biogeochemical timescale for the solute i.

P_i probability of consumption for the solute i.

N_i flux-weighted probability of consumption for the solute i $[\mathrm{LT}^{-1}]$.

References

Albarède, F. (1996), *Introduction to Geochemical Modeling*, 564 pp., Cambridge Univ. Press, Cambridge, U. K.

Angley, J. T., M. L. Brusseau, W. L. Miller, and J. J. Delfino (1992), Nonequilibrium sorption and aerobic biodegradation of dissolved alkylbenzenes during transport in aquifer material: Column experiments and evaluation of a coupled-process model, *Environ. Sci. Technol.*, 26(7), 1404–1410.

Arrigoni, A. S., G. C. Poole, L. A. K. Mertes, S. J. O'Daniel, W. W. Woessner, and S. A. Thomas (2008), Buffered, lagged, or cooled? Disentangling hyporheic influences on temperature cycles in stream channels, *Water Resour. Res.*, 44, W09418, doi:10.1029/2007WR006480.

Baker, M. A., C. N. Dahm, and H. M. Valett (1999), Acetate retention and metabolism in the hyporheic zone of a mountain stream, *Limnol. Oceanogr.*, 44(6), 1530–1539.

Bardini, L., F. Boano, M. B. Cardenas, R. Revelli, and L. Ridolfi (2012), Nutrient cycling in bedform induced hyporheic zones, *Geochim. Cosmochim. Acta*, 84, 47–61, doi:10.1016/j.gca.2012.01.025.

Bear, J. (1972), *Dynamics of Fluids in Porous Media*, Am. Elsevier, New York.

Bethke, C. M. (2008), *Geochemical and Biogeochemical Reaction Modeling*, 2nd ed., Cambridge Univ. Press, Cambridge, U. K.

Boano, F., C. Camporeale, R. Revelli, and L. Ridolfi (2006), Sinuosity-driven hyporheic exchange in meandering rivers, *Geophys. Res. Lett.*, 33, L18406, doi:10.1029/2006GL027630.

Boano, F., A. Demaria, R. Revelli, and L. Ridolfi (2010a), Biogeochemical zonation due to intrameander hyporheic flow, *Water Resour. Res.*, 46, W02511, doi:10.1029/2008WR007583.

Boano, F., R. Revellia, and L. Ridolfi (2010b), Effect of streamflow stochasticity on bedform-driven hyporheic exchange, *Adv. Water Resour.*, 33, 1367–1374, doi:10.1016/j.advwatres.2010.03.005.

Böhlke, J. K., R. C. Antweiler, J. W. Harvey, A. E. Laursen, L. K. Smith, R. L. Smith, and M. A. Voytek (2009), Multi-scale measurements and modeling of denitrification in streams with varying flow and nitrate concentration in the upper Mississippi River basin, *Biogeochemistry*, 93, 117–141, doi:10.1007/s10533-008-9282-8.

Boulton, A. J., S. Findlay, P. Marmonier, E. H. Stanley, and H. M. Valett (1998), The functional significance of the hyporheic zone in streams and rivers, *Annu. Rev. Ecol. Syst.*, 29, 59–81.

Boulton, A. J., T. Datry, T. Kasahara, M. Mutz, and J. A. Stanford (2010), Ecology and management of the hyporheic zone: stream–groundwater interactions of running waters and their floodplains, *J. N. Am. Benthol. Soc.*, 29(1), 26–40, doi:10.1899/08-017.1.

Brunke, M., and T. Gonser (1997), The ecological significance of exchange processes between rivers and groundwater, *Freshwater Biol.*, 37(1), 1–33.

Brusseau, M. L., L. H. Xie, and L. Li (1999a), Biodegradation during contaminant transport in porous media: 1. Mathematical analysis of controlling factors, *J. Contam. Hydrol.*, 37, 269–293, doi:10.1016/S0169-7722(99)00005-4.

Brusseau, M. L., M. Q. Hu, J. M. Wang, and R. M. Maier (1999b), Biodegradation during contaminant transport in porous media. 2. The influence of physicochemical factors, *Environ. Sci. Technol.*, 33(1), 96–103, doi:10.1021/es980311y.

Buffington, J. M., and D. Tonina (2009), Hyporheic exchange in mountain rivers II: Effects of channel morphology on mechanics, scales, and rates of exchange, *Geogr. Compass*, 3(3), 1063–1086, doi:10.1111/j.1749-8198.2009.00225.x.

Buffington, J. M., D. R. Montgomery, and H. M. Greenberg (2004), Basin-scale availability of salmonid spawning gravel as influenced by channel type and hydraulic roughness in mountain catchments, *Can. J. Fish. Aquat. Sci.*, 61, 2085–2096.

Buss, S., et al. (2009), *The Hyporheic Handbook: A Handbook on the Groundwater–Surface Water Interface and Hyporheic Zone for Environment Managers*, 280 pp., Environ. Agency, Bristol, U. K.

Cardenas, M. B. (2008a), Surface water-groundwater interface geomorphology leads to scaling of residence times, *Geophys. Res. Lett.*, 35, L08402, doi:10.1029/2008GL033753.

Cardenas, M. B. (2008b), The effect of river bend morphology on flow and timescales of surface water–groundwater exchange across pointbars, *J. Hydrol.*, *362*, 134–141, doi:10.1016/j.jhydrol.2008.08.018.

Cardenas, M. B. (2009a), A model for lateral hyporheic flow based on valley slope and channel sinuosity, *Water Resour. Res.*, *45*, W01501, doi:10.1029/2008WR007442.

Cardenas, M. B. (2009b), Stream-aquifer interactions and hyporheic exchange in gaining and losing sinuous streams, *Water Resour. Res.*, *45*, W06429, doi:10.1029/2008WR007651.

Chapelle, F. H. (2000), *Ground-Water Microbiology and Geochemistry*, 2nd ed., 496 pp., John Wiley, New York.

Dahm, C. N., N. B. Grimm, P. Marmonier, H. M. Valett, and P. Vervier (1998), Nutrient dynamics at the interface between surface waters and groundwaters, *Freshwater Biol.*, *40*, 427–451.

Drever, J. I. (1997), *The Geochemistry of Natural Waters: Surface and Groundwater Environments*, 3rd ed., 436 pp., Prentice Hall, Englewood Cliffs, N. J.

Estrella, M. R., M. L. Brusseau, R. M. Maier, I. L. Pepper, P. J. Wierenga, and R. M. Miller (1993), Biodegradation, sorption, and transport of 2,4-dichlorophenoxyacetic acid in saturated and unsaturated soils, *Appl. Environ. Microbiol.*, *59*(12), 4266–4273.

Fuller, C. C., and J. W. Harvey (2000), Reactive uptake of trace metals in the hyporheic zone of a mining-contaminated stream, Pinal Creek, Arizona, *Environ. Sci. Technol.*, *34*(7), 1150–1155, doi:10.1021/es990714d.

Gandy, C., J. Smith, and A. Jarvis (2007), Attenuation of mining-derived pollutants in the hyporheic zone: A review, *Sci. Total Environ.*, *373*, 435–446.

Ginn, T. R. (1999), On the distribution of multicomponent mixtures over generalized exposure time in subsurface flow and reactive transport: Foundations, and formulations for groundwater age, chemical heterogeneity, and biodegradation, *Water Resour. Res.*, *35*(5), 1395–1407.

Gu, C., G. M. Hornberger, A. L. Mills, J. S. Herman, and S. A. Flewelling (2007), Nitrate reduction in streambed sediments: Effects of flow and biogeochemical kinetics, *Water Resour. Res.*, *43*, W12413, doi:10.1029/2007WR006027.

Hester, E. T., and M. N. Gooseff (2010), Moving beyond the banks: Hyporheic restoration is fundamental to restoring ecological services and functions of streams, *Environ. Sci. Technol.*, *44*, 1521–1525, doi:10.1021/es902988n.

Hester, E. T., and M. N. Gooseff (2011), Hyporheic restoration in streams and rivers, in *Stream Restoration in Dynamic Fluvial Systems: Scientific Approaches, Analyses, and Tools*, *Geophys. Monogr. Ser.*, vol. 194, edited by A. Simon, S. J. Bennett, and J. M. Castro, pp. 167–187, AGU, Washington, D. C.

Hill, A. R. (1997), The potential role of in-stream and hyporheic environments as buffer zones, in *Buffer Zones: Their Processes and Potential in water Protection*, edited by N. Haycock et al., chap. 12, pp. 115–127, Quest Environ., Harpenden, U. K.

Hoehn, E., and O. A. Cirpka (2006), Assessing residence times of hyporheic ground water in two alluvial flood plains of the Southern Alps using water temperature and tracers, *Hydrol. Earth Syst. Sci.*, *10*, 553–563.

Hunter, K., Y. Wang, and P. Van Cappellen (1998), Kinetic modeling of microbially-driven redox chemistry of subsurface environments: Coupling transport, microbial metabolism and geochemistry, *J. Hydrol.*, *209*(1–4), 53–80.

Jiang, X.-W., L. Wan, M. B. Cardenas, S. Ge, and X.-S. Wang (2010), Simultaneous rejuvenation and aging of groundwater in basins due to depth-decaying hydraulic conductivity and porosity, *Geophys. Res. Lett.*, *37*, L05403, doi:10.1029/2010GL042387.

Jones, J. B., and P. J. Mulholland (Eds.) (2000), *Streams and Ground Waters*, Academic, San Diego, Calif.

Kasahara, T., and S. M. Wondzell (2003), Geomorphic controls on hyporheic exchange flow in mountain streams, *Water Resour. Res.*, *39*(1), 1005, doi:10.1029/2002WR001386.

Lamontagne, S., and P. G. Cook (2007), Estimation of hyporheic water residence time in situ using ^{222}Rn disequilibrium, *Limnol. Oceanogr. Methods*, *5*, 407–416.

Langmuir, D. (1997), *Aqueous Environmental Geochemistry*, 600 pp., Prentice Hall, Englewood Cliffs, N. J.

Lautz, L. K., and R. M. Fanelli (2008), Seasonal biogeochemical hotspots in the streambed around restoration structures, *Biogeochemistry*, *91*, 85–104, doi:10.1007/s10533-008-9235-2.

Li, L., I. Yolcubal, S. Sandrin, M. Q. Hu, and M. L. Brusseau (2001), Biodegradation during contaminant transport in porous media: 3. Apparent condition-dependency of growth-related coefficients, *J. Contam. Hydrol.*, *50*, 209–223.

Luo, W., and D. T. Pederson (2012), Hydraulic conductivity of the high plains aquifer re-evaluated using surface drainage patterns, *Geophys. Res. Lett.*, *39*, L02402, doi:10.1029/2011GL050200.

Marzadri, A., D. Tonina, A. Bellin, G. Vignoli, and M. Tubino (2010), Semianalytical analysis of hyporheic flow induced by alternate bars, *Water Resour. Res.*, *46*, W07531, doi:10.1029/2009WR008285.

Morrice, J. A., H. M. Valett, C. N. Dahm, and M. E. Campana (1997), Alluvial characteristics, groundwater-surface water exchange and hydrological retention in headwater streams, *Hydrol. Processes*, *11*, 253–267.

Morrice, J. A., C. N. Dahm, H. M. Valett, P. V. Unnikrishna, and M. E. Campana (2000), Terminal electron accepting processes in the alluvial sediments of a headwater stream, *J. N. Am. Benthol. Soc.*, *19*(4), 593–608.

Mulholland, P. J., et al. (2008), Stream denitrification across biomes and its response to anthropogenic nitrate loading, *Nature*, *452*, 202–206, doi:10.1038/nature06686.

Park, J., Y. M. Chen, J. J. Kukor, and L. M. Abriola (2001), Influence of substrate exposure history on biodegradation in a porous medium, *J. Contam. Hydrol.*, *51*, 233–256.

Peyrard, D., S. Sauvage, P. Vervier, J. M. Sanchez-Perez, and M. Quintard (2008), A coupled vertically integrated model to describe lateral exchanges between surface and subsurface in large alluvial floodplains with a fully penetrating river, *Hydrol. Processes*, *22*, 4257–4273, doi:10.1002/hyp.7035.

Pinay, G., T. C. O'Keefe, R. T. Edwards, and R. J. Naiman (2009), Nitrate removal in the hyporheic zone of a salmon river in Alaska, *River Res. Appl.*, *25*, 367–375, doi:10.1002/rra.1164.

Poole, G. C., and C. H. Berman (2001), An ecological perspective on in-stream temperature: Natural heat dynamics and mechanisms of human-caused thermal degradation, *Environ. Manage.*, *27*(6), 787–802, doi:10.1007/s002670010188.

Revelli, R., F. Boano, C. Camporeale, and L. Ridolfi (2008), Intra-meander hyporheic flow in alluvial rivers, *Water Resour. Res.*, *44*, W12428, doi:10.1029/2008WR007081.

Sawyer, A. H., M. B. Cardenas, and J. Buttles (2012), Hyporheic temperature dynamics and heat exchange near channel-spanning logs, *Water Resour. Res.*, *48*, W01529, doi:10.1029/2011WR011200.

Schneider, P., T. Vogt, M. Schirmer, J. Doetsch, N. Linde, N. Pasquale, P. Perona, and O. A. Cirpka (2011), Towards improved instrumentation for assessing river-groundwater interactions in a restored river corridor, *Hydrol. Earth Syst. Sci.*, *15*, 2531–2549, doi:10.5194/hess-15-2531-2011.

Schumm, S. A. (1985), Patterns of alluvial rivers, *Annu. Rev. Earth Planet. Sci.*, *13*, 5–27, doi:10.1146/annurev.ea.13.050185.000253.

Schumm, S. A., and H. R. Khan (1971), Experimental study of channel patterns, *Nature*, *233*(5319), 407–409, doi:10.1038/233407a0.

Storey, R. G., K. W. F. Howard, and D. D. Williams (2003), Factors controlling riffle-scale hyporheic exchange flows and their seasonal changes in a gaining stream: A three-dimensional groundwater flow model, *Water Resour. Res.*, *39*(2), 1034, doi:10.1029/2002WR001367.

Tompson, A. F. B., and K. J. Jackson (1996), Reactive transport in heterogeneous systems: an overview, in *Reactive Transport in Porous Media*, *Rev. Mineral.*, vol. 34, edited by P. C. Lichtner, C. I. Steefel, and E. H. Oelkers, chap. 6, pp. 269–310, Mineral. Soc. of Am., Chantilly, Va.

Tonina, D., and J. M. Buffington (2009), Hyporheic exchange in mountain rivers I: Mechanics and environmental effects, *Geography Compass*, *3*(3), 1038–1062, doi:10.1111/j.1749-8198.2009.00226.x.

Valett, H. M., C. C. Hakenkamp, and A. J. Boulton (1993), Perspectives on the hyporheic zone: integrating hydrology and biology. introduction, *J. N. Am. Benthol. Soc.*, *12*(1), 40–43.

Valett, H. M., J. A. Morrice, and C. N. Dahm (1996), Parent lithology, surface-groundwater exchange, and nitrate retention in headwater streams, *Limnol. Oceanogr.*, *41*(2), 333–345.

Valett, H. M., C. N. Dahm, M. E. Campana, J. A. Morrice, M. A. Baker, and C. S. Fellows (1997), Hydrologic influences on groundwater-surface water ecotones: Heterogeneity in nutrient composition and retention, *J. N. Am. Benthol. Soc.*, *16*(1), 239–247.

van den Berg, J. (1995), Prediction of alluvial channel pattern of perennial rivers, *Geomorphology*, *12*, 259–279, doi:10.1016/0169-555X(95)00014-V.

Varni, M., and J. Carrera (1998), Simulation of groundwater age distributions, *Water Resour. Res.*, *34*(12), 3271–3281.

Wondzell, S. M., J. LaNier, and R. Haggerty (2009), Evaluation of alternative groundwater flow models for simulating hyporheic exchange in a small mountain stream, *J. Hydrol.*, *364*, 142–151, doi:10.1016/j.jhydrol.2008.10.011.

Wroblicky, G. J., M. E. Campana, H. M. Valett, and C. N. Dahm (1998), Seasonal variation in surface-subsurface water exchange and lateral

hyporheic area of two stream-aquifer systems, *Water Resour. Res.*, *34* (3), 317–328.

Zarnetske, J. P., R. Haggerty, S. M. Wondzell, and M. A. Baker (2011a), Dynamics of nitrate production and removal as a function of residence time in the hyporheic zone, *J. Geophys. Res.*, *116*, G01025, doi:10.1029/2010JG001356.

Zarnetske, J. P., R. Haggerty, S. M. Wondzell, and M. A. Baker (2011b), Labile dissolved organic carbon supply limits hyporheic denitrification, *J. Geophys. Res.*, *116*, G04036, doi:10.1029/2011JG001730.

Zheng, C., and G. D. Bennett (2002), *Applied Contaminant Transport Modeling*, 2nd ed., 621 pp., Wiley-Interscience, Hoboken, N. J.